# Feasibility of Ambient Temperature Liquid Metal Air Batteries

A Major Qualifying Project Report

Submitted to the Faculty of the

Worcester Polytechnic Institute

in partial fulfillment of the requirements for the

Degree of Bachelor of Science

In

Chemical and Mechanical Engineering

Submitted by:

Ari Athair

Tristan Arnold

Date: May 18, 2020

Advisors: Ravindra Datta

Pratap Rao

Andrew Teixeira

# Acknowledgments

Our project would not have been possible without the guidance of others. We would like to thank the following individuals for their contributions to this project:

- **Professor Andrew Teixeira,** for guiding us and addressing any questions we had, plus allowing use of his lab and equipment.

- **Professor Pratap Rao,** for allowing the use of his potentiostat and lab space, as well as taking the time to go over new results.

- **Professor Datta Ravindra,** for advising us, sharing his sources as well as experience from past projects and research.

- The graduate students: Cameron Armstrong, Binod Giri, Heather LeClerc and Nicholas Pratt, for additional help in lab, setting up equipment and helping to answer questions as needed.

- **Worcester Polytechnic Institute** for providing us with the incredible opportunity to complete a Major Qualifying Project on a new type of energy storage.

# Abstract

With growing global electrification and rising impacts of greenhouse gasses, the demand for renewable energy rises. Inconsistent producers of energy (solar & wind) require improved energy storage. By using gallium, a nontoxic liquid metal at room temperature, we found a theoretical energy density 11 times commercial Li-ion, and kinetic performance superior to Zn-air batteries. Using cyclic voltammetry and testing of a prototype cell we reviled the reaction mechanism, proved the reversibility of gallium, and demonstrated rechargeability. We found improved rechargeability when adding 0.1M gallium oxide to 6M KOH electrolyte. However, short discharge times indicate limiting factors such as electrolyte drying still need to be addressed before commercial application.

# Authorship Page

| Section | Primary Author |
|---|---|
| Abstract | Ari Athair |
| 1.0 Introduction | All |
| 2.0 Literature Review | Ari Athair |
| 2.1 Current Energy Demand and Environmental Impact of Fossil Fuels | Ari Athair |
| 2.2 Storage methods | All |
| 2.2.1 Compressed air Storage | Tristan Arnold |
| 2.2.2 Types of Batteries | Tristan Arnold |
| 2.3 Electrochemistry of Gallium | Tristan Arnold |
| 2.3.1 Conflicting theories of Ga reaction mechanisms | Ari Athair |
| 2.4 Prior Work at WPI | Ari Athair |
| 2.5 Additional Relevant Work | Ari Athair |
| 3.0 Methodology | Ari Athair |
| 3.1 Potentiostat Testing | Ari Athair |
| 3.2 Swagelok Battery Test Cell Configuration | Ari Athair |
| 4.1 Findings from CV Testing | Ari Athair |
| 4.2 Electrodeposition Charge Test | Ari Athair |
| 4.3 Swagelok Cell Results | Tristan Arnold |
| 4.3.1 Polarization and Discharge kinetics | Tristan Arnold |
| 4.3.2 Charge/Discharge Cycles | Tristan Arnold |
| 4.3.3 Restricted Air flow with Varying Separators and Nitrogen Sparging | Tristan Arnold |
| 4.3.4 Calculations Evaluating the Quantity of KOH in Battery Tests | Ari Athair |
| 4.3.5 Calculations to Evaluate the Quantity of Ga Reacting in Prototype cell | Ari Athair |
| 4.3.6 Reaction Depth Calculations | Ari Athair |
| 5.0 Conclusions and Future work | All |

# Table of Contents

# List of Figures

# List of Tables

# 1.0 Introduction

The increasing global population, growing electrification and resulting dependence on energy is producing an ever-growing demand for electrical energy. In 2018, global energy demand rose by 2.3%, the fastest in the last decade, according to the International Energy Agency [17]. 70% of that growth was in the petroleum industry alone. The current main sources of energy production are imposing significant stresses on the environment. In 2018, energy related $CO_2$ production increased by 1.7% to 33 Gigatons, increasing global climate change impacts. Furthermore, energy demand is predicted to increase as a result of more frequent extreme temperature fluctuations linked to climate change. Currently energy production in the world is primarily based upon fossil fuel and nonrenewable resources which are the largest contributor to global energy related $CO_2$ production. In 2018, 89% of the energy production within the US was from non-renewable resources [23]. Within the United States the largest producer of greenhouse gas was the transportation industry in 2010 [8].

Renewable energy sources would address the energy demand and reduce global environmental impacts [18]. However, effective energy storage devices are limiting the wide scale spread and implementation of renewables. Effective storage methods are necessary to shift energy from intermittent production peaks from wind and solar generation to the times of high demand when the energy is needed. High energy dense storage is also necessary for the transportation industry to relinquish dependence on gasoline and to provide power sources small enough to progress technology further on an individual scale.

There are a few forms of energy storage that are promising to support the transition away from nonrenewable energy to more renewable sources, such as compressed air, kinetic energy

storage, thermal storage, fuel cells, capacitors, and batteries. Compressed air, kinetic energy, and thermal storage all require a large amount of space and are not portable. They can be effective for grid level storage but impractical for implication in the transportation industry as well as for small scales. Batteries have versatility in that they have a high energy density, typically are self-contained, have the potential of a high number of cycles and are more portable than the others, which would be a key aspect for implementation in transportation systems. Energy storage is also important for the implementation of rising "smart power grids" which will reduce help total consumption and energy costs [34]. Due to the current technology of batteries, and the growing energy demands most batteries are insufficient to store energy at a high enough energy density while maintaining rechargeability. To help solve this problem, advancements in batteries have led to higher energy dense configurations through experimenting with metal-air and liquid-metal batteries. There are many potential directions for batteries development that would help pave the way to higher energy storage in transportation and power grids around the world. The promising battery technology explored in this paper is the feasibility of a low temperature liquid metal air batter with a Gallium (Ga) anode.

New battery technologies are continually being researched today, with metal air batteries and liquid metal batteries having some of the highest theoretical energy densities identified. Air batteries only house half of the reactants, as abundant atmospheric oxygen is the second reactant. Metal air batteries are already implemented in some areas such as Zinc-air (Zn-air) hearing aid batteries, however some drawbacks come from the solid-gas interactions in these batteries, and the sluggish kinetics between the two. Liquid metal batteries have also been preliminarily researched due to their heightened kinetics and mass transfer capabilities associated with their liquid state along with their high energy density however, the melting points of most metals is so high that the

amount of energy stored and retrieved is reduced relative to the energy lost keeping the metals in a liquid state. Some companies have found ways to maintain the liquid state through self-generated heating during discharge and recharge, however this requires a special housing as the working temperature is >500$^{o}$C [16]. Another benefit of liquid batteries is the opportunity to configure them into a flow battery format which can easily increase their capacity to handle larger storage requirements, including at a grid scale. Liquid metal-air batteries are a comparatively new and unexplored concept. A liquid metal-air configuration would theoretically contain the benefits of both liquid metal and mental-air batteries while removing the shortcomings (Fig. 1) - the very high energy density of the solid metal-air while better reactivity kinetics and mass transfer properties due to the liquid state of these batteries [33]. Plus, the liquid state would prevent dendrite formation and battery shorting during repetitive recharge cycling, which has long been an issue in solid state batteries. During the initial work on this project Ga was chosen as the metal for its reactivity, low toxicity, and low melting point, which would allow it to function at near room temperature. Ga is one of few elements which are liquid at low temperatures and sufficiently reactive for this to be a feasible technology.

**Table 1.** Summary of how liquid metal air batteries would combine the benefits of liquid-metal and metal-air batteries.

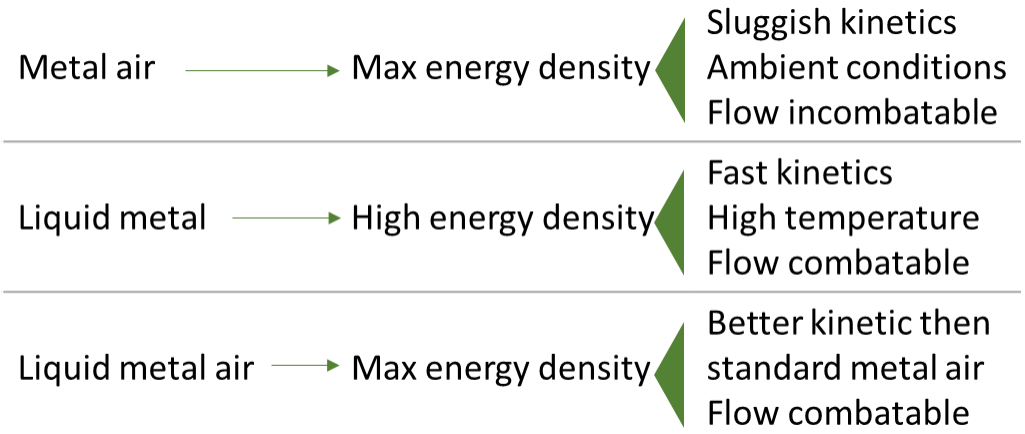

## 1.1 Objectives and Scope of the Project

The intent of this project was to continue the work of 3 prior Major Qualifying Projects (MQPs) by thoroughly investigate the limiting components and feasibility of recharging a liquid Ga-air battery. The previous work on this project gave a good launching point and showed potential, however some precursory analysis is necessary to evaluate the ability of Ga to charge and discharge. To evaluate this feasibility, measurements were taken using a potentiostat to test different electrolyte and electrode configurations to gain a better understanding of the fundamental chemical reactions occurring in the previous set up. Additionally, focus was directed towards the reducibility of the $Ga_2O_3$ skin as well as means to allow Ga to oxidize to completion. Evaluation of limiting factors and a deeper understanding of the stumbling blocks of past projects will preface development of a battery configuration designed to overcome the identified limitations.

# 2.0 Literature Review

In this section, we discuss the global energy demands, how current energy production is negatively impacting the environment, as well as how effective energy storage combined with renewable energy production can reduce that. We then discuss different energy storage methods and provide background information on current battery technologies. Finally, we will review relevant battery chemistries and the previous work that had been accomplished in relation to a liquid Ga air battery. This review expands upon key points mentioned in the introduction and provides background information for our research.

## 2.1 Current Energy Demand and Environmental Impact of Fossil Fuels

As the current energy demand is predicted to grow, greenhouse gas production is set to follow suite. Linked to the 2.3% increase in global energy demand in 2018 was a growth in natural gas consumption, coal and oil all contributing to a $CO_2$ production increase [17]. At the end of 2018 analysis showed that the global production had increased by 1.8% from the prior few years which had shown a plateau [5]. This is in part due to increased temperature variability and lower petroleum prices which have cause a higher consumption of energy. Prediction of the net production in 2019 by the Global Carbon Project indicates higher production likely this year as well [5]. The transportation industry has been the largest contributor to greenhouse gasses from 1990-2017 within the US. Composing 29% of the greenhouse gas emissions in the U.S.A. according to the Environmental Protection Agency while contributing to 14% production on a global scale [8]. The largest transportation related producer in the U.S. is small passenger transportation such as personal cars, trucks and minivans which make up for over half of transportation produced greenhouse gasses [8]. Unfortunately, the direction of $CO_2$ production is

moving in the wrong direction according to the Intergovernmental Panel on Climate Change's (IPCC) report on expectations of a 1.5$^{o}$C increase in global mean temperature relative to preindustrial standards. The IPCCs special report outlines that net global production of $CO_2$ would need to be reduced to 0 by 2050 for the global mean temperature to remain below this threshold [1]. Lowering emissions by 2030 significantly increases the chance that the global mean temperature will not surpass this threshold. According to the IPCC to maintain a global mean temperature rise of 1.5% or less renewable energy must supply a share of 52-67% of the primary energy while coal must decrease to 1-7% while still being paired with carbon capture storage [1]. Renewable dependence must be significantly increased for successful limitation of climate change.

According to the IPCC overshooting the 1.5$^{o}$C rise in global temperatures poses large risks for natural and human systems alike. Especially if the temperature at peak warming is high, some risks may be long-lasting and irreversible, such as loss of some ecosystems as well as irreversible melting of the permafrost on the geographical poles which would accelerate change to an unknown [1]. To prevent such a rise in global temperatures active steps to transition to renewable energy sources such as wind and solar, would reduce current $CO_2$ production are needed.

However, for an effective transition to renewables, a means of energy storage is necessary. Renewable energy production such as solar and wind have variable peak production times unrelated to periods of peak demand. Energy storage is necessary to shift energy from produced to times of peak use. Furthermore, application of energy storage systems is necessary for effective redistribution of power in smart grids which will reduce total consumption as well as decrease electrical costs at peak use times [34]. These developing smart grids store energy when demand and energy cost are low so it can be redistributed during times of peak use to lower the high costs of those times. The storage capacity necessary for smart grids also allows for reduced chances of

failure and back up energy supplies during outages as well a better adaptability to the growing number of small production systems that are being developed and incorporated to suburban homes, such as home solar installations [10]. For a storage system to be effective at a grid level extended discharge cycles would be a requirement as well as the ability to store a large amount of energy 1-500MW to supply the grid level demand [10]. Furthermore, such a storage device would need to have quick response from charge to discharge for quick adjustments can be effectively managed to either be stored for later or to be drawn. Figure 1 exemplifies the energy shift necessary for renewable energy such as Photovoltaic (PV) solar cells to be implemented into energy production.

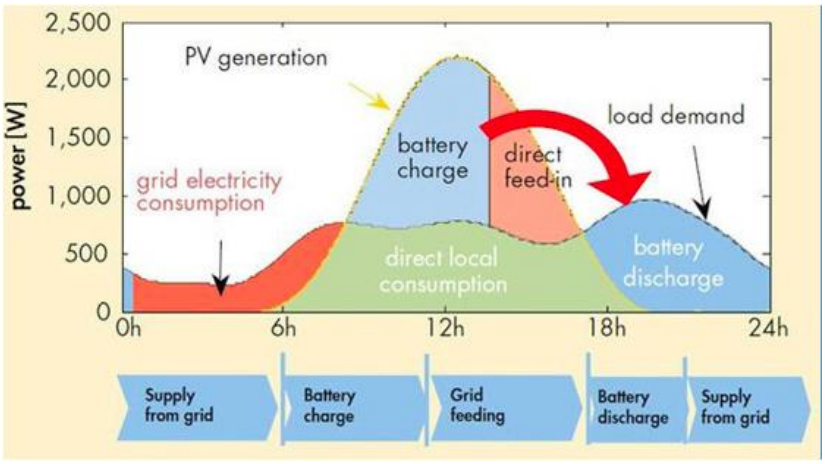


**Figure 1.** Solar energy shifting [26].

Furthermore, for renewable energy application in an industrial environment and in effective automobiles with a large radius of operation, a means of energy storage with a sufficiently high energy density is necessary. As transportation is one of the largest emitters of greenhouse gasses, increasing the energy density of rechargeable batteries would increase the usefulness of electric vehicles. Currently the tesla using lithium ion batteries can obtain a range of up to 325 miles on a single charge [28]. If a more energy dense battery is stabilized larger ranges would be achievable and application electric vehicles for industrial transportation would be attainable.

## 2.2 Energy Storage

Several methods of energy storage are being developed, each having pros and cons. The primary methods explored today are hydrogen storage in the form of fuel cells, mechanical methods such as kinetic energy (flywheels) and potential energy (pumped-storage hydropower, compressed air), thermal energy (ice, molten salts, steam) and electrochemical energy (batteries, flow cells) [24]. Figure 2 shows discharge times at rated power vs storage power rating of these storage methods can be compared.

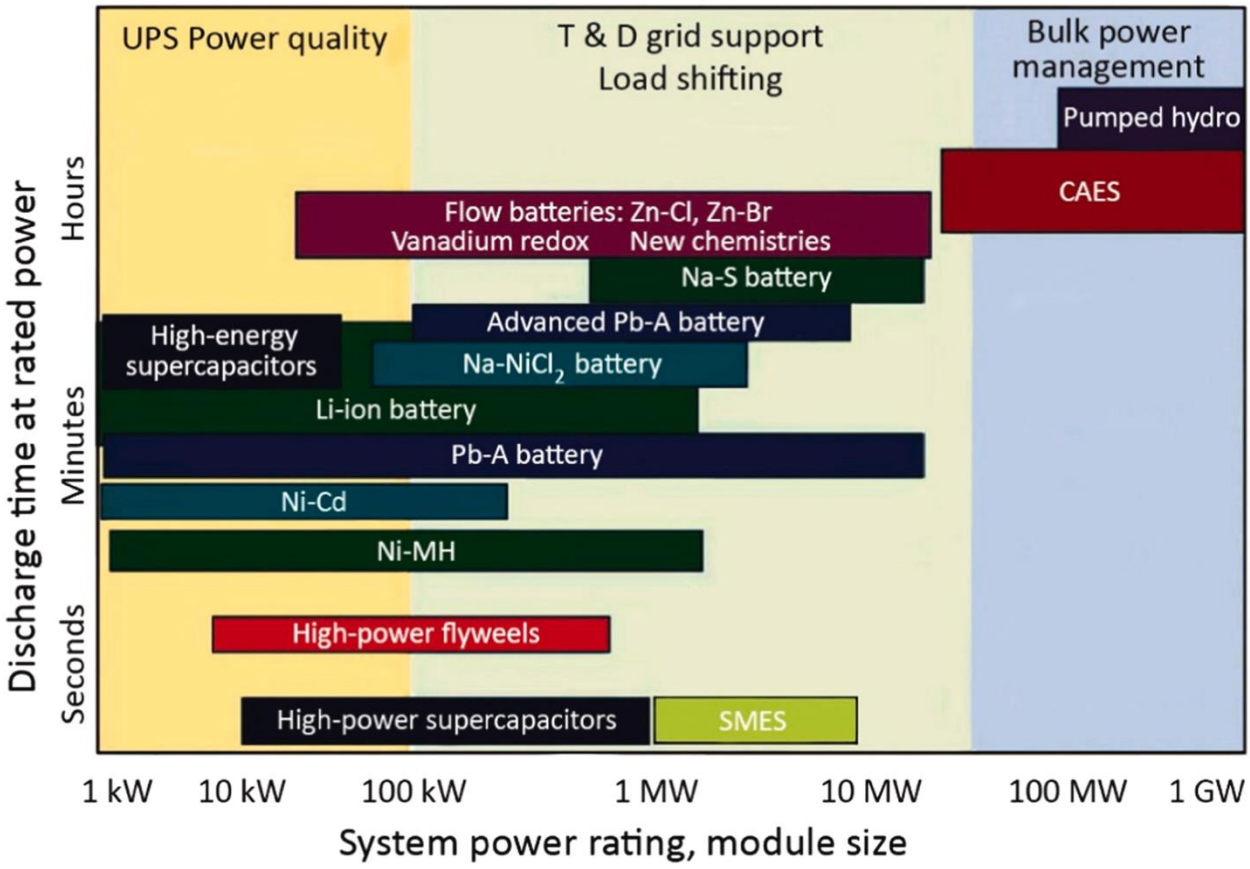


**Figure 2**. Comparison of different types of energy storage systems reproduced from Dehghani-Sanij et al., 2019 [27].

The integration of energy storage systems (ESS) is essential in maximizing energy efficiency and the overall performance of a network through the optimization of their placement, sizing, and operation. Current networks are at risk due to many factors including greenhouse gas emissions, demand, and the integration of renewable energies, such as wind and solar, and are having difficulty expanding to keep up with demand. The US Electric Power Research Institute, EPRI, has estimated that the annual cost of outages will reach upwards of $100 billion due to disruptions in these systems [4]. Therefore, ESSs are progressively being more and more implanted into current networks to offer safety as well as advantages to improve power quality, load shifting, and peak shaving, among others, to relieve problems posed by oscillations in power usage and abrupt changes and interruptions to systems currently in place. One such ESS is compressed air energy storage.

### *2.2.1 Compressed air Storage*

Due to current integrated storage technologies having trouble meeting all the electricity demand, some countries, such as Denmark, have started integrating compressed air energy storage (CAES) into their power grids. Currently, in Denmark, wind power accounts for only 20% of the demand with combined heat and power (CHP) following with 50%, however this still only totals to less than 75% of the energy demand which can, and has, lead to excess electricity production problems. CAES, as it stands, is one of the highest economically feasible technologies and may help create an energy system that can better utilize the differing output of the renewable energies mentioned. This system employs a modified gas turbine where low-cost electricity is used to store the compressed air underground. Then, the air is heated and expands within the turbine to produce electricity during peak demand hours [14].

Although the storage systems put in place have been improving the energy storage of alternative energies and other energy producing plants, batteries are still one of the more ideal solutions to the problem. Since their initial discovery in the late 1700s, they have improved by being less environmentally invasive and have decreased in size while maintaining their electronic potential. With this in mind, their ability for portability is unmatched, which is ideal for supplying power for the transportation industry however, they only have so much charge so having them be rechargeable and energy dense for storage and for grid scale would help alleviate some of the problems with energy demand.

### *2.2.2 Types of Batteries*

All batteries work due to redox reactions. Redox reactions, short for reduction-oxidation, is a type of chemical reaction in which electrons between two atoms are exchanged, changing their oxidation states, with the reducing agent losing electrons and the oxidizing agent gaining electrons. This transfer of electrons, in turn, creates a current which, depending on the atoms involved, can create a certain voltage. In a standard Galvanic cell, there are two electrodes, the cathode and anode, an electrolyte, and a separator. These cells are designed as to isolate both half reactions of a redox reaction and allow excess electrons to build up at the negative electrode, the cathode, and create an electron “vacuum” at the positive electrode, the anode. Then the electrons can cross from one electrode to the other when they are connected via a conductor so that the cell can do work.

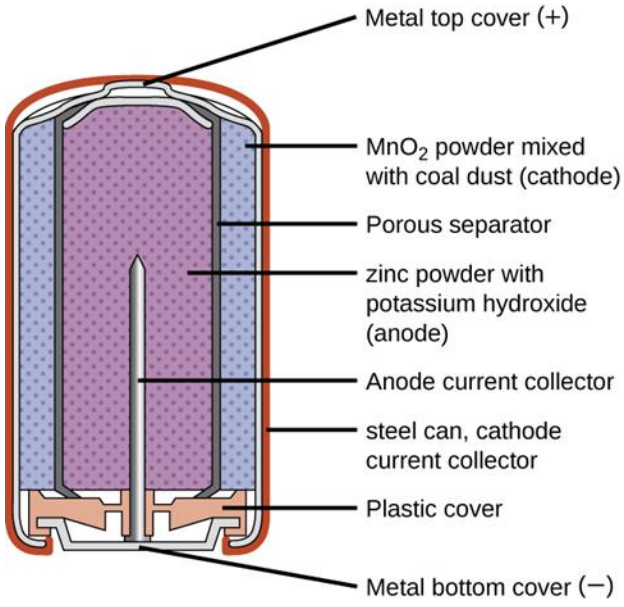


**Figure 3.** Diagram of a galvanic cell battery [6].

In this diagram, the Zn powder in the center, surrounded by a porous separator, allows ions to pass through, while the Manganese Oxide in the outer layer surrounds the Zn core but is restricted by the separator to prevent mixing.

All batteries can be put into one of two categories, primary or secondary. With Primary batteries, the electrochemical reaction is non-reversible and are designed to be only used once before discarding. On the other hand, Secondary cells are rechargeable and involve redox reactions that can be reversed using electricity such as Lead-acid, Nickel-Cadmium and Lithium-ion. Secondary batteries, also known as rechargeable batteries, are batteries in which the cell is based on electrolysis and are aptly named electrolytic cells. This battery achieves rechargeability by applying a reverse current which causes ions to flow in the opposite direction back into their initial state thus recharging the cell. These batteries have the advantage of being more cost-efficient over the long term however, per unit, they are more costly and generally have a lower capacity and

lower voltage [22]. This in mind, finding a way to create a secondary battery with the electronic potential of other batteries, it would be a viable solution to the power grid crisis arising.

The traditional battery as most people are aware is the lithium-ion battery. This battery, as useful and universal as it may be, has certain drawbacks. Due to their popularity and continued use, lithium deposits have slowly been depleted over the past which leads to them being a rarity and, as such, more expensive as well as there being continued issues with dendrite formation shorting batteries remains and issue. Although many advances are being made to remedy these obstacles, Researchers are looking to other, alternative batteries with comparable energy densities at a similar, or less, cost.

One iteration of the standard galvanic cell is the Redox Flow Battery (RFB). With this battery, there are two reactants with an electrolyte separator and consist of two vessels for holding discharged or charges electrolytes, something to convert the energy, usually a cell stack which is comprised of different cells running in series/parallel, pumps and the connection to the generating/consuming device. An example schematic is shown in Fig. 4.

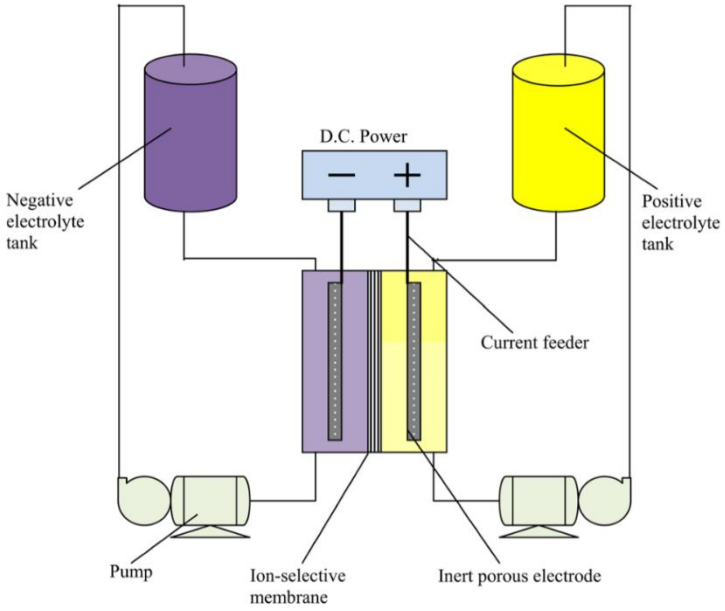


**Figure 4.** Schematic of a Standard RFB [21].

The main benefit to this style of battery is that they can easily be scaled in size and capacity for use in power grids however, the current chemistry behind the RFB does not allow for particularly high energy densities which could be rectified by combining the mechanics of the RFB with the electrochemistry of batteries like the metal-air or liquid metal.

Metal-air batteries are batteries are unique in the sense that the cathode active material, which is often oxygen in the air, does not have to be stored in the battery, but rather can be accessed from the surrounding ambient oxygen. These metal-air batteries which utilize either alkali or alkaline metals as the anode present very appealing due to their potential of having very high energy densities. The metal-air battery with the most appeal is the Lithium-air (Li-air) because the discharge reaction has a voltage of 2.91V as well as a theoretical specific energy of 5200 Wh/kg including oxygen and 11140 Wh/kg excluding it [11].

## 2.3 Electrochemistry of Gallium

In one experiment conducted in the 1950's, the electromotive forces were measured on different cells involving Ga such as Ga chloride and Ga perchlorate with its Hydrogenated counterpart at different temperatures spanning 20°C to 35°C. These measurements were made at different gallic ion concentrations and different acidities. Through testing, the standard electrode potential of Ga was found to be -0.560 ± 0.005 volts with the standard free energy at 25°C to be -38,800 cal/mol-°C as well as the standard entropy and enthalpy to be -39.2 cal/mol-°C anode -50,500 cal/mol respectively [3].

Von Bergkampf, found that the potential for the two gallic cells to be -0.53 V, assuming the activity coefficients of Ga were equal to those of lanthanum (1953). He also found that the potential of Ga electrodes that were prepared under hydrogen varied vastly initially but became stable after two to four days. Over the course of the experiment conducted by Saltman and Nachtrieb, the potentials suddenly dropped about 300 mv when Ga melted and remained at that lowered value as the liquid Ga super-cooled until 26°C, at which point, the potential rose sporadically to almost its original value [3].

### *2.3.1 Conflicting Theories of Ga Reaction Mechanisms in Alkali Solutions.*

To gain a better understanding of the reactions taking place at a given pH for an electrochemical system the Pourbaix diagram is often studied. As a physical representation of the Nernst equation the Pourbaix diagram of Ga in an aqueous environment (Fig. 5) indicates what reactions are likely taking place during oxidation and reduction at a given pH.

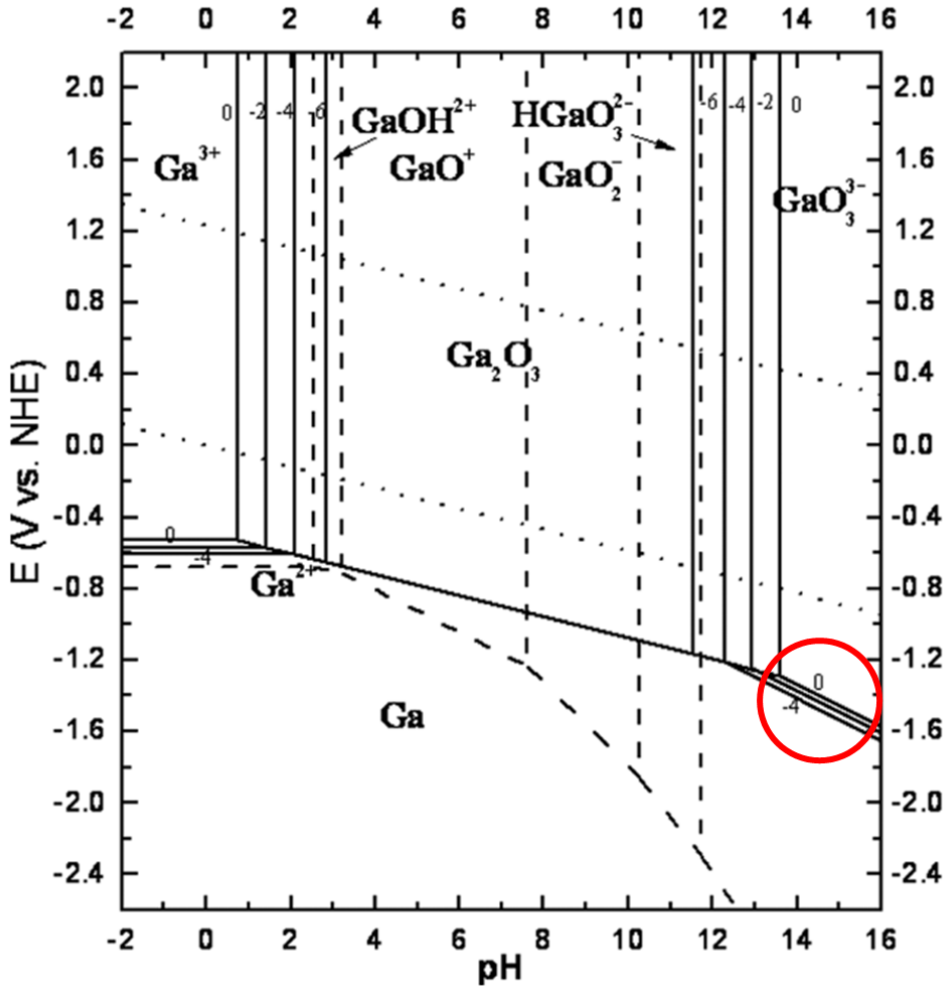


**Figure 5.** Potential (V vs NHE)-pH equilibrium diagram for aqueous systems of Ga at 25C [12].

The region of interest for Ga oxidation and reduction is contained within the red circle as this region pertains to the pH of 6M KOH the electrolytes investigated by this work. According to Pourbaix [12] , equations which apply to this region are net reactions across multiple lines and can be seen below.

Solubility of $Ga_2O_3$:

$$\mathbf{Ga_2O_3} + 3\,H_2O = \; 2GaO_3^{---} + 6H^+ \qquad \log(GaO_3^{---}) = -40.81 + 3\,pH$$

Potential of Ga at high pH:

$\mathbf{Ga} + 3\,H_2O = \; GaO_3^{---} + 6H^+ + 3e^-$ $\qquad E_0$= 0.319-0.1182pH+0.0197log($GaO_3^{---}$)

Combining these two equations at a pH of 14.78 (6M KOH with maximal solvation of $Ga_2O_3$ gives $E_0$= -1.358 V vs SHE or -0.485 V vs RHE

Reference electrode conversion: V vs RHE = 0.0591*14.78+V vs SHE

Comparison to these values will be further discussed in section 4.1.3.

The work of Pourbaix is a good starting point but when evaluating the reactions taking place and expected products formed in alkali Ga redox reaction, the literature is inconsistent. Some past researchers disagree whether mono a bivalent state of Ga exist during the reactions and if they are stable. Additionally, in the application to a battery cell with limited aqueous electrolyte the resulting product is unknown, though likely a mix of dissolved $Ga_2O_3$ and $Ga(OH)_3$ films. In table 2. the reaction pathways according to different theories has been summarized to show the differences.

**Table 2**. Potential reaction pathways according to literature.

| **Theory** | **Reaction Pathway** |
|---|---|
| Suggests stable ionic species of Ga(III) in solution to be of the form $H_2GaO_3^-$ . With rate controlled is by the Ga(II)-Ga(III) redox step with assumption that Ga(II) has stability in alkali solution (Bockris and Enyo, 1962). | $Ga + 2OH^- \leftrightarrow GaO^- + H_2O + e^-$<br>$GaO^- + OH^- \leftrightarrow HGaO_2^- + e^-$<br>$HGaO_2^- + OH^- \leftrightarrow H_2GaO_3^- + e^-$<br>total:<br>$Ga + 4OH^- \leftrightarrow H_2GaO_3^- + H_2O + 3e^-$<br>With unstable Ga(I) dissociation<br>$3GaO^- + 2H_2O \leftrightarrow 2Ga + H_2GaO_3^- + 2OH^-$<br>Or<br>$HGaO_2^- + GaO^- + H_2O \leftrightarrow Ga + H_2GaO_3^- + OH^-$ |

| | |
|---|---|
| Proposed intermediary valent steps, however in these steps Ga(II) as a transient intermediate only. Considering Ga(II) instability in alkali solutions disagreeing with Bockris and Enyo (T. HURLEN, 1963) | $Ga + 2OH^- \leftrightarrow Ga(OH)_2^- + e^-$ fast<br>$Ga(OH)_2^- + OH^- \leftrightarrow Ga(OH)_3^- + e^-$ slow or fast<br>$Ga(OH)_3^- + OH^- \leftrightarrow Ga(OH)_4^- + e^-$ slow or fast<br>Total:<br>$Ga + 4OH^- \leftrightarrow Ga(OH)_4^- + 3e^-$ |
| Expected 3 electron transfer in $OH^-$ solutions of concentration greater than 1M [12]<br>Primary Oxidation peak matches 3e transfer either Ga2o3 or GaOH3 surface reaction formation (Varadharaj & Rao, 1990) | $2Ga + H_2O \leftrightarrow Ga_2O_3 + 2H^+ + 6\,e^-$<br>$Ga_2O_3 + 3H_2O \leftrightarrow 2GaO_3^{3-} + 6H^+$<br>Total:<br>$Ga + 3H_2O \leftrightarrow GaO_3^{3-} + 6H^+ + 3e^-$ |
| A2, anticipated oxidation reaction for second peak, non-reversible unstable monovalent Ga(I) formation quickly decomposes to metallic and trivalent forms (Varadharaj & Rao, 1990). | $2Ga + H_2O \leftrightarrow Ga_2O + 2H^+ + 2\,e^-$<br>$Ga_2O + 2H_2O \leftrightarrow Ga_2O_3 + 4H^+ + 4e^-$<br>$3\,Ga_2O \xrightarrow{\text{disproportionate}} 4Ga + Ga_2O_3$<br>$2Ga + 3H_2O \leftrightarrow Ga_2O_3 + 6H^+ + 6\,e^-$ |
| Pathway (I) stable ions formed and no surface films.<br>Pathway (II) $Ga(OH)_3$ is produced at low concentrations (2a)<br>At high concentrations passivating layer is formed with background cation ($K^+$) (2b)<br>Pathway (III) Ionization under conditions of direct electrosynthesis of passivating electrode surface film (Korshunov, 1995) | Pathway(I)<br>$Ga + 4OH^- \leftrightarrow Ga(OH)_4^- + 3e^-$<br>Pathway (II)<br>$Ga \leftrightarrow Ga^{3+} + 3e^-$<br>$Ga^{3+} + 3OH^- \leftrightarrow Ga(OH)_3$ (2a)<br>$K^+ + Ga(OH)_4^- \leftrightarrow K[Ga(OH)_4]$ (2b)<br>Pathway(III)<br>$Ga + (x + 2y)OH^-_{ads} \leftrightarrow [Ga(OH)_xO_y]^{(x+2y-3)-}_{ads} + yH_2O + 3e^-$ |
| Incorporates individual fast single electron transfer in hydroxide reaction and similar pathways to well understood Zn-air batteries. (WPI MQP, 2015) | $Ga + 4OH^- \leftrightarrow Ga(OH)_4^- + 3e^-$<br>$Ga\,(OH)_4^- \leftrightarrow Ga(OH)_3 + OH^-$<br>$Ga(OH)_3 \leftrightarrow Ga_2O_3 + H_2O$<br>Total: $Ga + 3OH^- \leftrightarrow \frac{1}{2}Ga_2O_3 + \frac{3}{4}H_2O + 3e^-$ |

Though there is variation in the above reaction pathways they agree that Ga completes its reaction in a trivalent state. Though the final states may be either oxides or hydroxides. In the

actual battery application - opposed to surplus electrolyte solution where most of these tests were run - there is a limited amount of aqueous basic electrolyte and oxides are more likely to be the final product with surplus oxygen for reacting.

Two additional reactions of importance are consistent throughout the literature and are shown in table 3. These two reactions are the $H_2$ evolution pathway with Ga present and the cathode 4 electron reduction of $O_2$.

**Table 3.** Other reactions taking place.

| Reaction | Pathways |
|---|---|
| $H_2$ evolution pathway (Selekhova, Lyubimova, and Leikis, Elektrokhimiya, 1972) Similar to Zn-Air $H_2$ evolution pathway according to comparison with [2] | $Ga + OH^- \leftrightarrow Ga(OH) + e^-$<br>$Ga(OH) + OH^- \leftrightarrow Ga(OH)_2^-$<br>$Ga(OH)_2^- + 2H_2 \leftrightarrow [Ga(OH)_3]^- + 2H_2$ |
| 4 electron pathway for $O_2$ Cathode reaction of high pH air batteries [2] | $O_2 + 2H_2O + 4e^- \leftrightarrow 4OH^-$ |

## 2.4 Prior Work at WPI

Three past MPQs researched and tested a liquid Ga-air battery in 2015, 2016 and 2017, however there is still a notable gap to be filled in their work. The MQPs validated that a Ga-air type battery could work and obtained consistent discharges from their test cells, however little success was met when attempting to recharge the test cells. It is unknown if Gallium oxide ($Ga_2O_3$), the product, is easily reduced and recharged in the traditional sense by applying a reverse charge to prototype battery. Additionally, the limiting reactants of the prototype cell are still unknown. It is hypothesized that electrolyte carbonization of KOH may be the limiting factor, however $H_2O$ due to electrolyte drying as well as self-limiting $Ga_2O_3$ may be reducing the discharge and energy density of the prototype cell. In the past projects there has been little study of the foundational electrochemical reaction present in this test cell, as well as what would be necessary for an

effective rechargeable cell with this chemical composition. An understanding of Ga, $Ga_2O_3$ and as well as the limiting factors, on a basic chemical level is needed before rechargeability and a more effective cell can be assembled to overcome past pitfalls.

### *2.4.1 Work Achieved by the 2015 MQP*

In 2015, Tyler Howard, Laura Merrill & Stephen Johnston established a proof of concept for a liquid Ga air battery through a flat constant current discharge as well identifying some of the limiting factors of the test set up that was used. The main interest of this battery development was to determine the feasibility of a liquid metal air flow battery. However, to first validate the proof of concept, a prototype Swagelok cell design was used to test the feasibility of a Ga-air electrochemical cell without the addition of a flow system. This prototype lacks the dynamics of a flow configuration in that it is composed of static layered configuration. Flat discharge time of the test cell for over 10hr with constant current drain at 50-60$^oC$ and open circuit voltage ranging from 1.1-1.4 V was measured in the initial test cell. Comparable to those of commercial Zn-Air batteries which provided a potential of 1.4V. Discharge and polarization performance was also analyzed at various temperatures and compared to theoretical values as well as the commercial Zn air batteries. Pure Ga was used as the anode, along with a 6M potassium hydroxide aqueous electrolyte soaked in a Zirconia (Zr) cloth separator and platinum-catalyzed gas diffusion layer (GDL) to help improve $O_2$ reaction kinetics. Despite the success the capacity of the test cell was much lower than that of the Zn-Air cell. Some of the hypothesized limiting factors that the project proposed were "electrolyte carbonation, separator drying, and oxide layer formation" which would have decreased the capacity relative to the theoretical values. Theoretical calculations and analysis of the Ga reactions were performed and yielded theoretical potentials given below however it was

unknown if $Ga_2O_3$ or $Ga(OH)_3$ was the resulting product of the reaction so both calculations were performed. Table 4 and 5, show the resulting calculations.

**Table 4**. Thermodynamic Voltage vs SHE for Gallium Hydroxide Product, Reproduced from [7].

| **Electrode** | **Reaction** | **Potential (V)** | $\Delta G^o$ **(kJ/mol)** |
|---|---|---|---|
| Anode | $Ga + 4OH^- \leftrightarrow Ga(OH)_4^- + 3e^-$ | | |
| Anode | $Ga(OH)_4^- \leftrightarrow Ga(OH)_3 + OH^-$ | | |
| Overall anode | $Ga + 3OH^- \leftrightarrow Ga(OH)_3 + 3e^-$ | $E^o = -1.242$ V | -360 |
| Cathode | $O_2 + 2H_2O + 4e^- \leftrightarrow 4OH^-$ | $E^o = 0.401$ V | -155 |
| Overall | $Ga + \frac{3}{4}O_2 + \frac{3}{2}H_2O \leftrightarrow Ga(OH)_3$ | $E^o = 1.643$ V | -476 |

**Table 5.** Thermodynamic Voltage vs SHE for Gallium Oxide Product, Reproduced from [7].

| **Electrode** | **Reaction** | **Potential (V)** | $\Delta G^o$ **(kJ/mol)** |
|---|---|---|---|
| Anode | $Ga + 4OH^- \leftrightarrow Ga(OH)_4^- + 3e^-$ | | |
| Anode | $Ga(OH)_4^- \leftrightarrow Ga(OH)_3 + OH^-$ | | |
| Anode | $Ga(OH)_3 \leftrightarrow Ga_2O_3 + H_2O$ | | |
| Overall anode | $Ga + 3OH^- \leftrightarrow \frac{1}{2}Ga_2O_3 + \frac{3}{4}H_2O + 3e^-$ | $E^o = -1.323$ V | -383 |
| Cathode | $O_2 + 2H_2O + 4e^- \leftrightarrow 4OH^-$ | $E^o = 0.401$ V | -155 |
| Overall | $Ga + \frac{3}{4}O_2 \leftrightarrow \frac{1}{2}Ga_2O_3$ | $E^o = 1.724$ V | -499 |

Tests of potential vs current density were measured for Zr and AEM which revealed carbonation may be limiting reaction at lower potentials. Polarization curves of Ga-air and Zn-air were compared and showed the Zn outperformed the prototype cell in all aspects. A large

contributor of this is hypothesized to be the contact area of the anode with the electrolyte; in the Ga cell only small contact is made between the Ga and KOH, while Zn powder is mixed with KOH in the anode compartment allowing for maximum direct contact between the anode and electrolyte material in the Zn battery.

Theoretical calculations were made of the discharge capacity of Zn-Air and liquid Ga-air resulting in a 40% higher value for Ga via use of the following two equations.

$$E_Q = \frac{nF}{3600 * MW_{anode}} \left[\frac{Ah}{g}\right]$$

$$t = \text{Discharge service Life [h]} = \frac{Q[mAh]}{\text{discharge current [mA]}}$$

The gravimetric and volumetric energy density of Ga-air, by hydroxide and oxide formation and Zn-Air was calculated presenting a higher value for both Ga reactions, the resulting comparison in table 6.

**Table 6.** Theoretical energy density of Ga-air batteries reproduced from [7]

| Electrochemical System | Gravimetric Energy Density (Wh/kg) | Volumetric Energy Density (Wh/L) |
|---|---|---|
| Zn-air | 1,361 | 9,723 |
| Ga-air ($Ga(OH)_3$) | 1,895 | 11,549 |
| Ga-air ($Ga_2O_3$) | 1,989 | 12,121 |

This calculation however did not include the required amounts of electrolyte necessary for Ga-air reactions to progress which would result in some inaccuracy. Variation of test configuration

and comparison to theoretical polarization curves found that Zr cloth was preferable of the tested anode separators and electrolyte interface materials [7]. However, the Zr separator was Ga permeable resulting in wetting Ga through into cathode container which shorted the batteries. Temperature variation showed optimal operating temperature to be 55$^{o}$C and testing in a pure $O_2$ vs atmospheric conditions showed no conclusive change in results.

### *2.4.2 Work Achieved by the 2016 MQP*

During the 2016 MQP, the group worked to improve the battery set up from the year before by testing different electrolytes as well attempting to assess rechargeability [20]. The tests were geared to reduce impacts of electrolyte drying and carbonization which were the projected limiting factors from the prior project. Tests with Ga droplets mixed in KOH gelled with PVA (polyvinyl alcohol), resulted in "inconsistent and inconclusive" discharge times [20]. However, when using two KOH soaked Zr Separators increased the discharge time to a consistent 25 hrs, when compared to using a single separator which discharged for only 10-12 hrs. The use of an alumina cloth separator was also tested without conclusive improvement. A temperature study of the dual separator cell and resulted in similar yields to the prior years' work. With the longest discharge times at~50$^{o}$C however the second longest times were at 40$^{o}$C and discharge times drastically diminished at higher temperatures of 70$^{o}$C. Their explanation was that the placement of the temperature probe was closer to the actual temperature of the test cell. Exemplified by the Ga maintaining its liquid form when taking the cell apart while in the prior year, at the 40$^{o}$C tests the Ga was solidified when disassembling the test cell, indicating that the actual test temperature was lower than the probe indicated [20]. Polarization curves were also analyzed at these different temperatures and indicated a similar higher efficiency at the lower temperatures 40-60$^{o}$C and lower efficiency at 70$^{o}$C. Further testing of re-wetting and soaking showed some additional discharge,

indicating that with two soaked separators $OH^-$ was still a critical limiting component of the reaction. This indicated that carbonation may be a key reason that limits discharge duration and performance [20]. An 8M KOH electrolyte was also tested however the 6M results outperformed it on all levels. Lastly, preliminary evaluation of rechargeability was researched relative to a commercial NiMH battery, however no effective recharge was observed. $MnO_2$ was tested as a potential replacement for the platinum catalyzed GDL for rechargeability however it showed negligible improvement. This can likely be attributed to the presence of $H_2O$ in the aqueous electrolyte, because the theoretical voltages necessary to reverse $Ga_2O_3$ in to its anodic state are higher than the voltage necessary for electrolysis, hydrogen evolution and oxygen evolution which would prevent recharging effectively while simultaneously drying out the available electrolyte.

### *2.4.3 Work Achieved by the 2017 MQP*

During the 2017 project the same Swagelok prototype was used for further testing, the work of the prior projects was reproduced and elaborated upon. X-ray diffraction was used to identify the products formed by the battery cells reaction. Through this, it was found that $Ga_2O_3$ was the product of this test cell. Five different electrolytes were tested on the assembly from past projects to evaluate more options, these included potassium hydroxide, Ga nitrate, $Ga_2O_3$, tetrabutylammonium chloride hydrate and tetrabutylammonium ammonia hydroxide. The last two being ionic liquids.

Furthermore, tests were performed with a Ga-tin alloy of 92-8% by weight composition. This alloy showed promise as it provides a lower cost as well as a more stable and increased, discharge at the optimal temperature assessed to be $60^oC$. Addition of $Ga_2O_3$ into the electrolyte was evaluated for positive impact and was found to be beneficial. Different concentration of $Ga_2O_3$

addition was evaluated and showed the maximum benefit was observed at a concentration of 0.17M $Ga_2O_3$ [20].

Tetrabutylammonium ammonia hydroxide was tested and showed some promise. A long discharge life was observed; however, a lower yield voltage was obtained due to Ga leaking through the Zr separator and shorting the configuration, some additional separator configurations were tested without success.

When an aqueous electrolyte was used no success was met while attempting to charge the Ga air cell, both in the initial cell and in the form of a $Ga_2O_3$-electrolyte slurry. However, when using the ionic liquid which showed some success during discharge tests (tetrabutylammonium ammonia hydroxide), some discharges of 20minutes and 40minutes were observed after charging which showed that there may be potential for rechargeability in a non-aqueous composition battery cell. To overcome the shortcomings of past projects finding a superior electrolyte separator to prevent Ga transfer through the separating and shorting the battery is necessary with the uses of this ionic liquid electrolyte, as well as evaluation of further non-aqueous electrolyte configurations for a rechargeable cell to be developed.

**2.5 Additional Relevant Work**

One study conducted by the Dickey research group may have some relevance to a Ga air battery. A method for controlling the interfacial energy (surface tension) of liquid Ga was presented, through electrochemical removal of surface oxides [32]. According to this study placing oxidized Ga in a strong acid or base with $10<PH<3$ and concentrations higher than 0.1M will automatically cause dissolution of the surface oxide layer [31]. A Ga indium alloy was primarily used for the studies however the results were said to be consistent for pure Ga above its melting

point. In an acid or base Ga will wet a copper wire which was used as the connecting electrode [31]. When the Ga is oxidized via application of a positive voltage the $Ga_2O_3$ acts a surfactant and decreases the high surface tension present in the pure Ga droplets [31]. A voltage is applied to the working electrode and a counter electrode within the electrolyte, voltages of >1 is applied for small changes in surface tension while a voltage <1 cause larger change in surface deformation as well as movement towards the counter electrode.

When conducting a reduction experiment oxidized Ga was placed in a neutral electrolyte with 1M concentration such as NaF or NaCl. A negative voltage greater than 1 V is then applied to the Ga causing the oxide to completely reduce into its metallic state [31]. It was noted, not to surpass the voltage which causes hydrogen evolution (-1.23 V at standard conditions), causing the electrolyte will degrade and the reduction of Ga to be restricted. This investigation indicates it is possible to apply a voltage less than that calculated as necessary in past MQP (-1.323 V) to reduce $Ga_2O_3$. Additionally, this research gives insight into the ability of Ga to oxidize and reduce, as well the impact of the electrolyte PH on this reaction, impacting the decision of an optimal electrolyte which will facilitate rechargeability.

Another study of the “Self-Actuation of Liquid Metal via Redox Reaction” [25], using Galinstan (an alloy of Ga) provides further indirect findings relevant to a Ga-air battery. The Galinstan was placed in a small anodic glass chamber and submerged in NaOH. a copper electrode is connected to the Galinstan and external to the cell. Copper also acts as a counter electrode reacting with $O_2$ which passes through a permeable silicone membrane at the opposite end of a fluidic channel. Making an external electrical connection between the two copper electrodes results in a spontaneous redox reaction with oxidizing and oxygen reducing like the intended Ga air battery chemistry [25]. NaOH dissolves the oxide film as it grows on the Galinstan allowing for

the dramatically lower interfacial tension, initiating a metal flow into the channel. As the metal flows new Galinstan is exposed allowing for an unhindered redox reaction to progress. When the external connection is broken, NaOH causes dissolution of the remaining $Ga_2O_3$ returning ambient surface tension which pushes the Galinstan back into the anodic chamber via capillary pressure [25]. This setup and progression can be seen in Fig. 6.

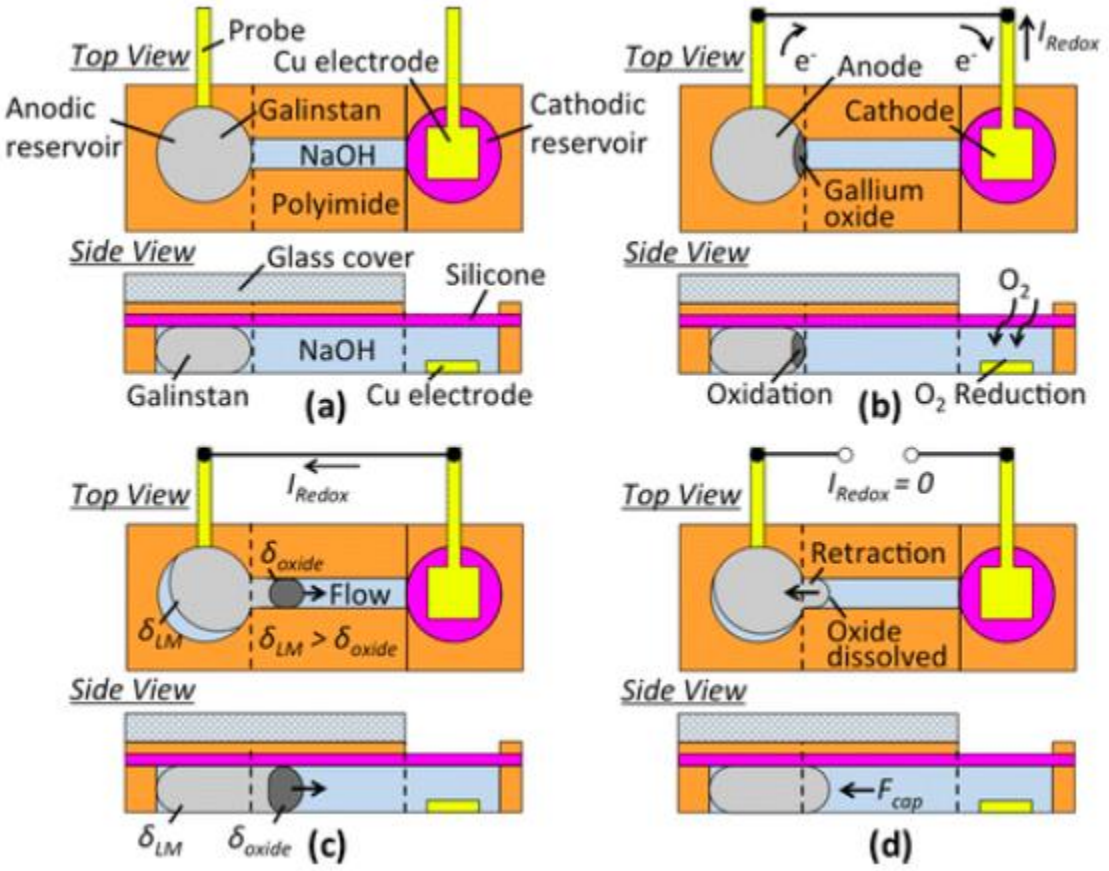


**Figure 6.** Self-actuating micro capillary Ga battery [25].

a) denotes the ambient configuration of the test cell. b) Shows the initial changes as an external connection is made allowing for a redox reaction to begin. c) Shows how the oxide formation allows for flowing into the connecting channel, localized interfacial tension is denoted by δ. d)

Shows how the oxide is dissolved and Ga retracted into the anodic chamber when the external connection is severed.

This test cell was quite small and provided currents of ~110 μA. However, higher concentration of the electrolyte resulted in larger currents as a result of the increased rate of dissolution of the $Ga_2O_3$. Copper was used for its low cost and conductivity however the high PH of the solution caused degradation of the metal, indicating that improvement should be made for further testing. Theoretical evaluation of the recharge life of the tested cell "estimate a device lifetime of over 9000 cycles before the Galinstan loses its eutectic properties" [25]. This study provides further insight into the potential uses of electrolytes for reducing as well as the benefits of flow and capillary forces in the development of a Ga-air battery. These ideas will be considered for our development of a new Ga-air battery.

# 3.0 Methodology

The goal of our project was to further the research of prior MQP's towards the development of a rechargeable liquid Ga-air battery. Development of this type of battery would be a new step in battery development and energy storage. To accomplish this goal two main objectives were developed by our team.

1. The analysis of the fundamental electrochemical reactions to determine ability of Ga to recharge, as well as limiting factors of the Swagelok prototype configuration.
2. Modification of test cell based on findings to overcome identified limitations.

## 3.1 Potentiostat Testing

Due to the redox nature of batteries, one method commonly employed for fundamental electrochemical analysis is Cyclic Voltammetry (CV) using a potentiostat. CV is a method used to investigate the reduction and oxidation process of molecular species by applying a voltage difference in a pyramid wave form and measuring the resulting current. As a result of these experiments a graph is created, referred to as a voltammogram, shown in figure 6. The shape and values of characteristic variables can be used qualitatively to evaluate the reversibility of a redox reaction.

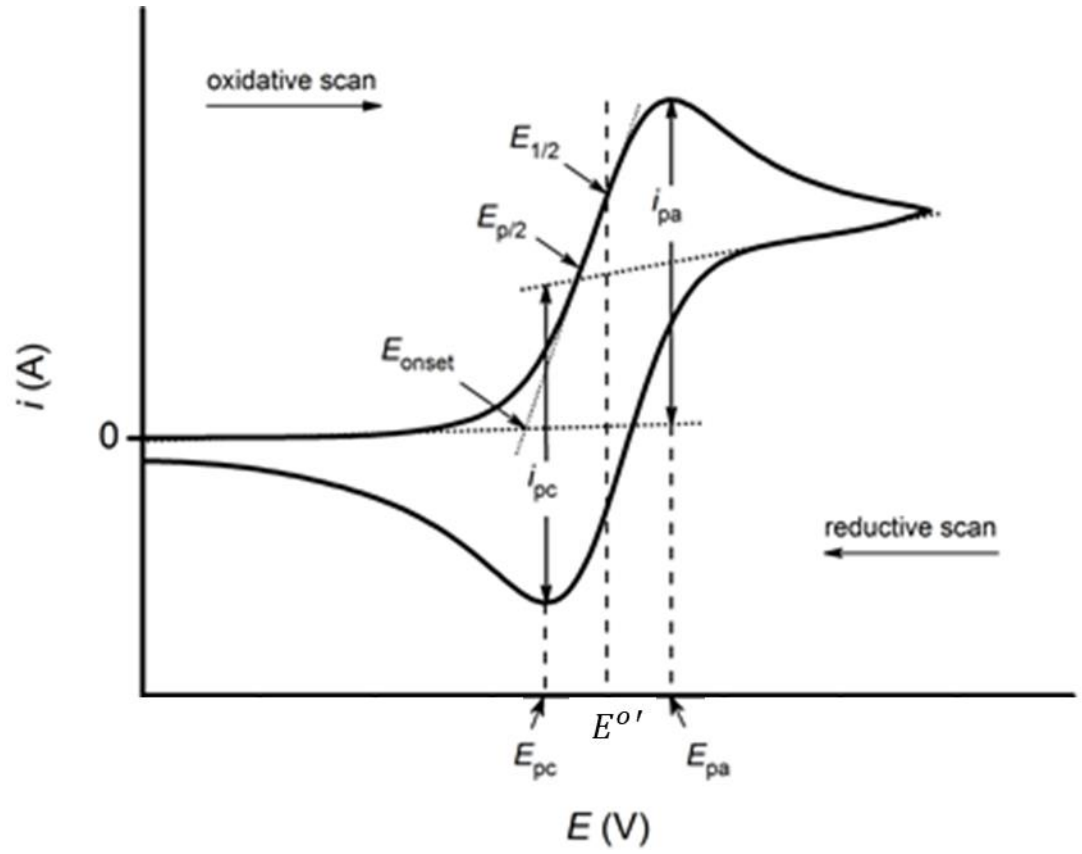


**Figure 7.** Reversible CV curve with important variables [19].

Voltammograms show the imposed parameter, voltage on the x-axis, with the corresponding dependent value, current or current density on the y-axis with the arrows indicating the direction in which the potential was scanned. The top peak corresponds with oxidation and is referred to as the anodic/oxidation peak where the lower peak at Epc is the reduction peak. This shape is indicative of reversible reactions in CV and commonly referred to as the "duck" shape. It describes the equilibrium reached through the Nernst equation, which relates the potential of an electrochemical reaction to the standard reduction potential of the redox reaction. Within these kinds of experiments, the scan rate is important because it controls how fast the applied potential is scanned. Faster scans lead to a decreased size of the diffusion layer and, as a result, higher currents are observed. For certain electrochemically reversible redox, the Randles-Sevcik equation

describes how the peak current increases linearly with the square root of the scan rate. This equation can help indicate whether an analyte is freely diffusing in the solution. (Elgrish et. al, 2018).

### *3.1.1 CV Testing Methodology*

Cyclic Voltammetry (CV) was used to develop an understanding of the underlying fundamental chemistry taking place in this battery configuration. A three-electrode cell was used. Composed of a working electrode (Ga in this case), counter electrode, which provides an electrical opposite, and a reference electrode used to quantify the varying voltage. This experimental technique was chosen because it is one of the most "popular technique for initial electrochemical studies of new systems and has proven very useful in obtaining information about fairly complicated electrode reaction" [13]. By varying the scan rate the diffusion coefficient of this system may be evaluated which can provide insight on whether the electrochemical system is diffusion or kinetically limited or if limitations are based on other factors. CV testing also allows evaluation of the systems rechargeability, to see if the Ga to $Ga_2O_3$ reaction is reversible, quasi reversible or irreversible and therefore if this type of battery can be recharged.

To conduct cyclic voltammetry tests, a potentiostat made by Bio-Logic scientific instruments with model number SP-200 was used. This was connected to a lab desktop which data was collected on through EC-Lab V11.31 supporting software. Results were analyzed within the EC-Lab as well within MS Excel for later analysis. Set up and programs which were run can be seen in Appendix A & B.

All test configurations used a Standard Cadmium Electrode (SCE) made by Gamry Instruments (part number 930-00003) as reference electrode. Voltages measured were later

converted from SCE to RHE (Reversible Hydrogen Electrode) as this is a more widely used reference electrode particularly in solutions of variable pH. Additionally, zero voltage relative to the RHE electrode denotes the point at which hydrogen evolution begins. This is an important reaction and relative location to be aware of as hydrogen evolution may cause limit the effectiveness of the electrolyte. Two different counter electrodes were tested, both Nickle wire and a graphite rod. Four different working electrode connections to Ga were also tested. Stainless Steel sheet metal, Pt catalyzed carbon cloth GDL used in the past battery tests, insulated copper electrical wire and lastly an insulated Pt wire.

To convert from SCE to RHE the conversion below was used

$$RHE = SCE + 0.241 + 0.0591 \times PH$$

Before voltages may be converted the pH of the electrolyte solution must be tested or calculated.

$$14 = pH + pOH$$

Calculating the pH of 6M KOH gives:

$$pH = 14 - (-\log[6]) = 14.78$$

Which gives $RHE = SCE + 1.1145$

The diagram below shows the relation between voltage, pH, and electrolysis of water, the hydrogen evolution reaction. Following the lower line one can see that as pH increases the voltage needed to induce hydrogen evolution decreases which will be further discussed in relation to this project later.

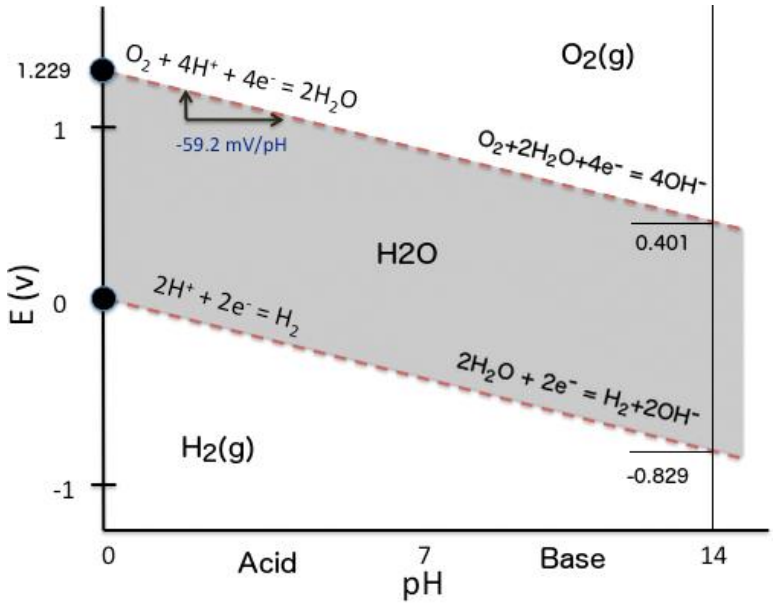


**Figure 8.** Oxygen and hydrogen potential depending on pH [12].

### *3.1.2 Analysis with EC-Labs*

Some of the key metrics for analysis of the CV results are $E_{p/2}$, $E_{pc}$, $E_{pa}$, $I_{pa}$, $I_{pc}$, shown in Fig. 9. Because a regression line is needed to obtain $I_{pa}$ and $I_{pc}$ from the data, these values were obtained using the "Peak Analysis" function in EC-Labs. The desktop curser is used to select the data points surrounding the peak and the system automatically analyzes the peak current as well as the half current and related potentials of each. In the diagram bellow one can see how the different variables relate, and how the software analyzes the results. Either a linear or polynomial regression line can be used to measure the peak current relative too, however all values in this report were extracted using the linear setting.

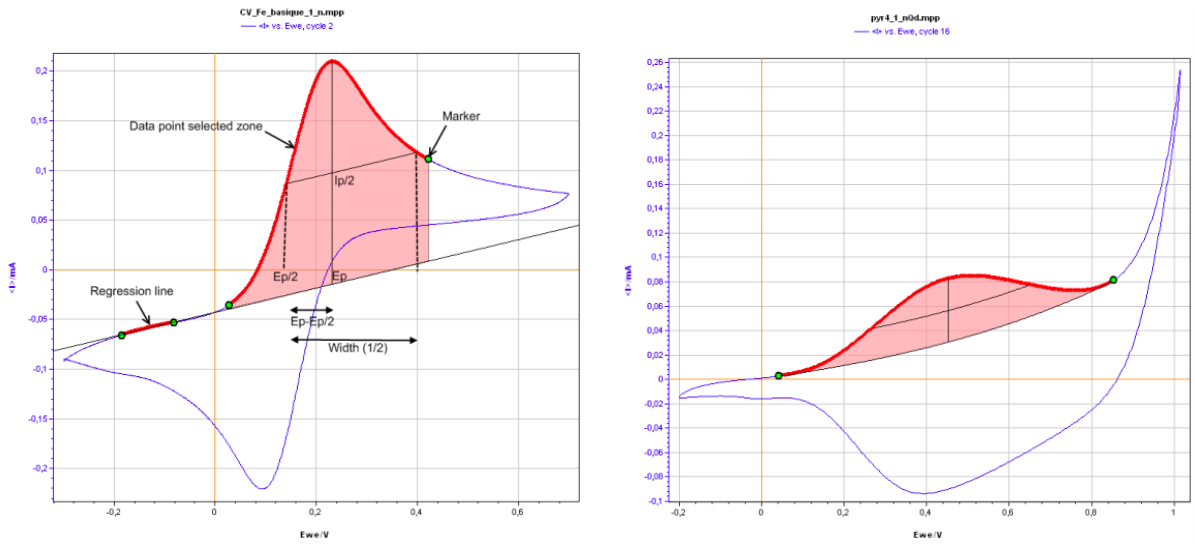


**Figure 9.** Diagram showing peak analysis within EC-Labs [30].

**Left** shows linear regression line method for analysis of the wave peak values. **Right.** Polynomial regression line analysis. Both examples show oxidation peaks (the upper/forward peak) analysis however the same process is applied for the reduction peak as well.

Although CV testing tends to give a more qualitative understanding of the background chemical reactions there are some quantitative characteristics which can be observed which denote reversible reactions (Bard, & Faulkner, 2001). Four main details are mentioned in literature which characterize the reversibility of electrochemical electron transfer in CV results and voltammograms. These were used for evaluation of reversibility of results.

- First the peak current ratio should be near unity for reversible reactions [29].
- Second, the mid peak potential should not very significantly with changing scan rate [35].

- Thirdly, for reversible systems peak anodic and cathodic currents should vary linearly with the square root of the scan rate for reversable systems due to the Randles–Sevcik relation $i_p = (2.69 \times 10^5)\, n^{\frac{3}{2}} A\, D_o^{\frac{1}{2}} C_o^* \nu^{\frac{1}{2}}$ [15].

- Forth, the peak separation should approximately follow the relation of Epa-Epc = 59mV/n (Krishnan, 2011), however the experimental values rarely fit this and so it is often disregarded. The key part of this last point is that the peak potentials should remain constant and independent of the scan rate for a reversible system.

Additionally, the equation $\left|E_p - E_{p/2}\right| = 2.20 \times \frac{RT}{nF} = \frac{56.5}{n}\,\text{mV at } 25^{o}\text{C}$ can be used to evaluate the number of electrons "n" transferred for a given peak.

### 3.2 Swagelok Battery Test Cell Configuration

The prototype battery setup can be used to reproduce the Ga-air battery developed by Howard, et al. [7] and further adapted by Hu, et al. [20] and Marx & Raposa [9]. Additionally, testing of modifications to this cell can be conducted to consider the results of previous experimentation. Figure 10 shows the exploded view of the basic test configuration which was inverted during tests to allow for greater contact between the liquid Ga and the electrolyte separators.

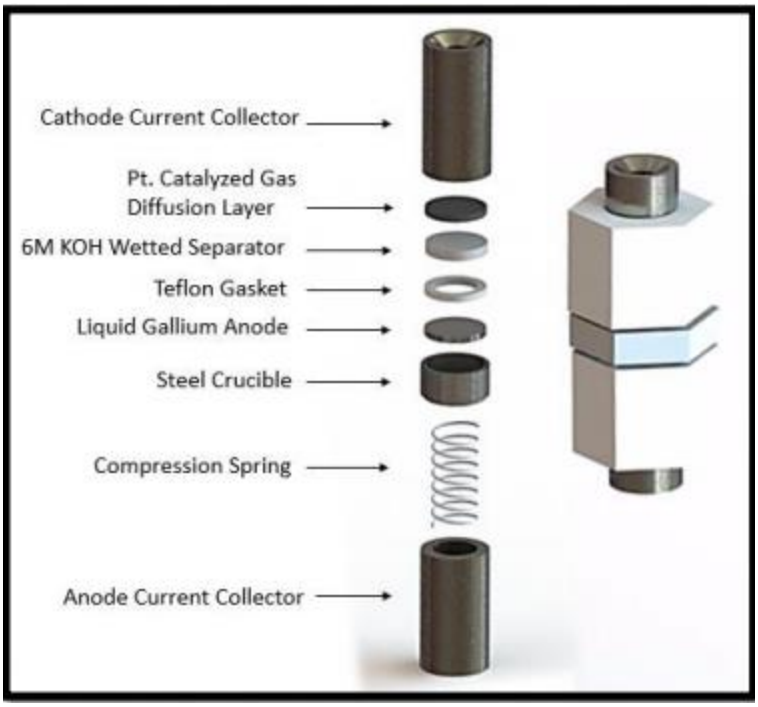


**Figure 10.** Schematic for the original Swagelok cell [7].

Experiments which were run include, varying the number of battery separators, and changing the order of different types of separators (Zr and polypropylene) within the cell. Additionally, tests were run with $N_2$ sparging through cathode to evaluate oxygen dependence. As well as with a sealed airless environment to evaluate if the flow was drying the electrolyte. All test were run with 6M KOH electrolyte however some were run with additional quantities of $Ga_2O_3$ dissolved in to the electrolyte.

### *3.2.1 Materials*

The mechanical parts and initial assembly followed previous projects [7], [20], [9]. Stainless steel cathode and anode current collector manufactured by Target Machine 36. Stainless steel crucible to hold Ga anode machined by WPI Machine shop. McCaster Carr 302 stainless steel

precision compression spring, spring (0.750 in. long, 0.36 in. O.D., 0.026 in. thick wire). PTFE Swagelok tube fitting with ferrules, union, 0.5 in. tube O.D.

Nonmechanical components include a platinum catalyzed carbon GDL to improve reaction kinetics between $O_2$ and the electrolyte. This was the same GDL used by past MQPs, "LT40EW Low Temperature ELAT GDE microporous layer including 5g/m2 Pt electrode on woven web made by Pemeas Fuel Cell Technologies" [7]. The battery separators used for result reproduction was a Zircar woven cloth type ZYK-15 (yttria-stabilized Zr), with a thickness of 0.3048 mm (0.012 inches) and a porosity of 85 %. These separators were fabricated by using a 1.4 cm diameter hole punch. 25um thickness, 2500 Celgard polypropylene separators were also tested and were made using the same 1.4 cm hole punch. An electrolyte of 6M 33.6% KOH wt (33.6g /100mL DI water) was used to wet all the separators and was the most effective electrolyte used in past projects. Teflon gasket was used to seal between layers with inner diameter of 0.9cm and outer diameter of 1.4cm. Ga of 99.999% purity purchased from Alfa Aesar by previous project was used as the anode of test cell. As well as $Ga_2O_3$ obtained from sigma Aldrich which was added to the electrolyte for some tests.

## 3.3 Battery Analyzer

Once battery assembly was completed, tests were run using a BA500WIN Battery Metric analyzer. The battery metric model used is a modified MC2020 which is capable of measuring and charging at low discharge currents and voltages. This was the same battery analyzer as used by the prior three MQPs [7], [20], [9]. A small external fan was also used to prevent overheating of the battery metric as the internal fan is broken as found by Marx & Raposa [9]. The battery metric was

run in parallel and controlled via software program BA500WIN Ver 1.38 installed on a lab computer.

Different programs were imputed into the BA500WIN depending on the desired test. The "Battery Type" chosen will be "Primary (Non-Rechargeable)" when the battery is solely being discharged, while "Nickel-Cadmium battery" will be selected when the battery was being charged. For both situations only 1 battery cell is selected and rated at 1,000 mAh capacity as in the past MQPs [7]. To reproduce past results, the same base case run was used. This was composed of a 20-minute pause followed by a galvano-staircase polarization curve, 15-minute pause, 0.5 mA discharge and finishing with a 20-minute pause. This script is run continuously, until a discharge cutoff voltage of 0.1V was reached. The galvano-staircase polarization curve measured the voltage of the battery at incremental increases of current from 0 mA to 7.5 mA in 0.1 mA increments every 20 seconds (0.33 minutes). Once the current reached 7.5 mA, 0.5 mA incremental increased occurred every 20 seconds, until a current of 15 mA was reached [7]. After the galvano-staircase polarization curve, a 15-minute pause allows the battery to recover from the polarization curve. After which, a constant current was applied to fully discharge the battery. In the base case, a current of 0.5 mA was used. The battery metric however can allow discharges anywhere from 0.5 mA to 3 mA. After the battery voltage dropped below 0.1V, a 20-minute pause allowed the battery to stabilize so an ending open-circuit voltage can be determined. This same program was used for a nitrogen sparge test and a limited air flow test. Additionally, a charge/discharge plot was created with a program consisting of a stabilizing initial 10-minute pause step followed by 60 minute, 5mA discharge/charge cycles with a 0.1 V cutoff for the discharge steps. With each of these programs, the cell was set underneath a heat lamp to ensure an average cell temperature of 50 °C.

# 4.0 Results and Analysis

## 4.1 Results from CV Testing

During CV test several different test configurations were tried to find one which gave the best results. The initial test configuration used a small piece of stainless-steel sheeting bent in such a manner that it would hold the Ga droplet in the small dimple created, this acted as the working electrode. A nickel wire was used as counter electrode initially. Irregular results were observed. This can be due to the exposed area of the steel reacting with the solution as well as large observed electrolysis. The nickel counter electrode may also have caused some variability, as it is somewhat reactive with the electrolyte solution, as a result a graphite rod was used to replace the Ni wire to have a less reactive counter electrode.

### *4.1.1 Copper Wire tests*

An insulated copper electrical wire was used to connect to the Ga. The insulation was removed at the two tips so that electrical connection to the Ga droplet could be made. The counter electrode and reference electrodes remained the same. Initially this worked well, as copper has good wetting properties with Ga at this high pH, however changes in Ga surface tension as voltage was applied, made it impossible to maintain electrical contact between the electrical wire and Ga throughout cycling and resulted in the lower irregular results depicted in figure 11.

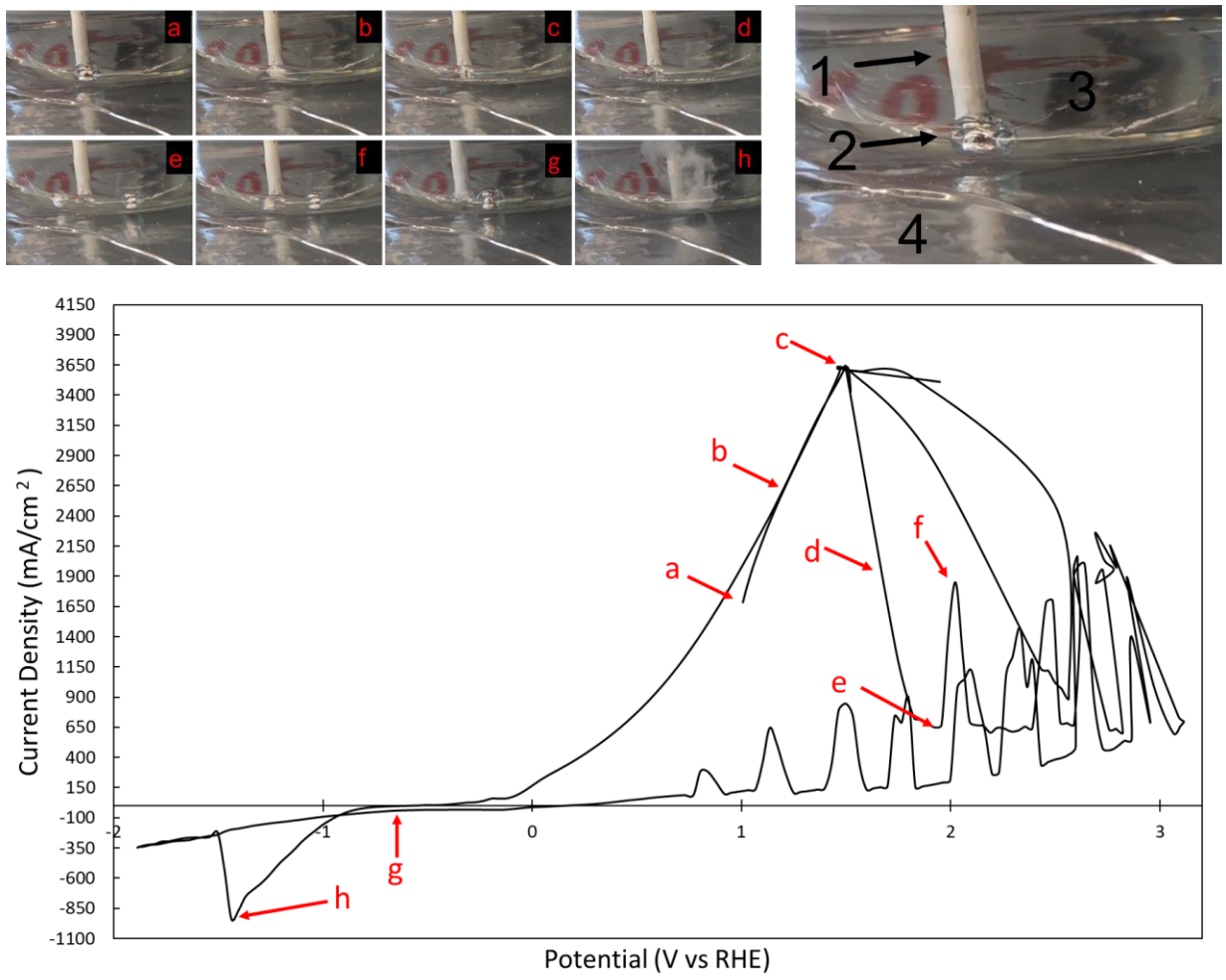


**Figure 11.** Voltammogram showing impact of changing surface tension of unrestricted Ga, copper electrode connected to Ga in KOH.

In the images above one can see the effects of voltage on the surface tension of the unrestricted Ga droplet corresponding to changing voltage and current in the voltammogram. (1) Corresponds to the white insulated wire connecting to the Ga droplet. (2) Ga droplet. (3) 6M potassium hydroxide (KOH) electrolyte solution in a beaker. (4) Hot plate to maintain liquid state of Ga. Initially at voltage (a) the droplet is at rest with the natural surface tension of Ga holding it into a spherical shape. As a positive voltage is applied (b, c, d) $Ga_2O_3$ forms acting like a surfactant to remove the surface tension until finally it spreads out so much the electrical connection between electrode and Ga is severed (d, e). Once the electrical connection is lost the Ga regains its strong surface tension

springing back into spheres. Because the side of the beaker, which had the electrode, was at the lowest point the Ga droplets rolled back into contact with the electrode and lost surface tension again (e, f, g) this resulted in current spiking until the cycling voltage lowered to the point that the surface tension did not decrease (g). Once the voltage reached a low enough point hydrogen evolution takes place creating the bubbles and spike at location (h).

These changes in surface tension made it very difficult to get a clear reading and consistent connection between the connecting electrode - the insulated copper electrical wire - and the Ga droplet throughout each cycle. As a result, no quantifiable data could be extracted. The addition of a plastic pouch or non-reactive plastic Swagelok valve cap, to contain the Ga droplet within the beaker provided usable results. The container within the beaker contained the Ga as the surface tension changed allowing for constant electrical connection between the Ga and connecting copper wire electrode throughout CV tests. In figure 13. below the results can be seen with the Ga connected to a Copper electrical wire (insulated except for the portion in contact with Ga and external potentiostat electrode). Containing the Ga within the solution allowed constant connection to be maintained while surface tension fluctuated. Care was taken to make sure the electrolyte was at a sufficiently high level for unrestricted contact between the Ga and other electrodes. The resulting voltammogram shows a slight “duck shape” which is looked for during investigations of redox rechargeability.

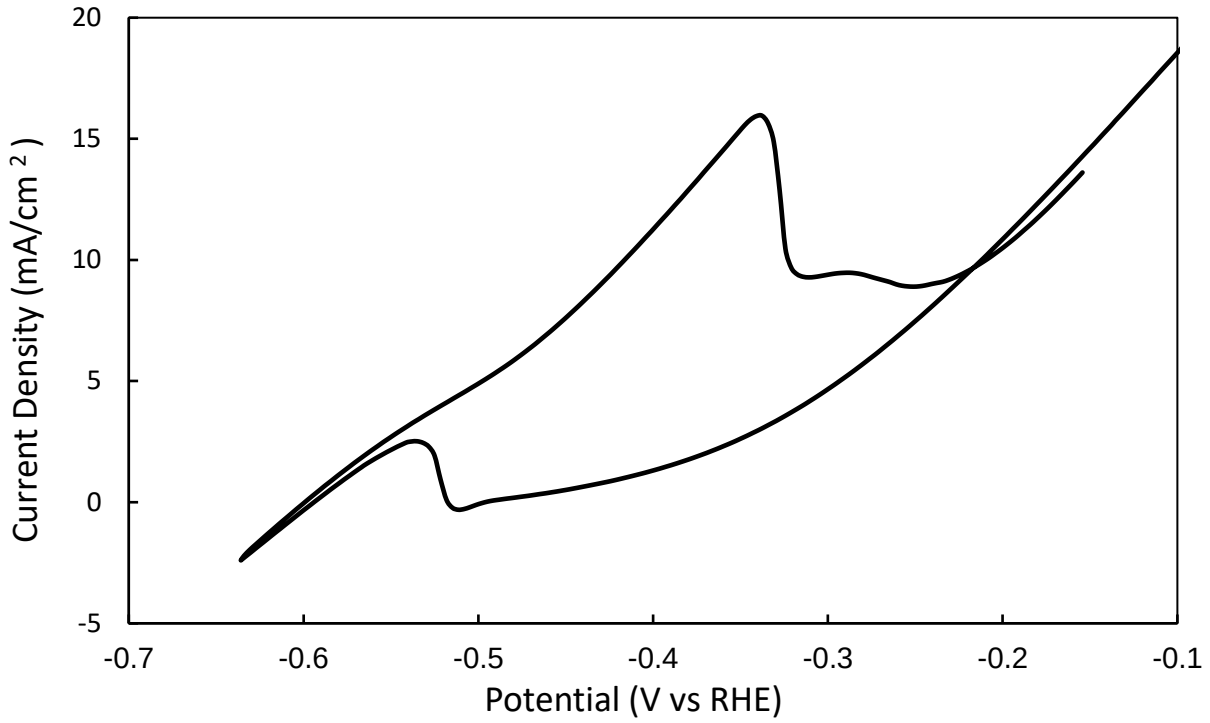


**Figure 12.** Voltammogram of copper connected to contained Ga in 6M KOH.

The two peaks are located at ~ -0.4246 ± 0.0869 (V vs RHE). The oxidation peak also appeared markedly larger than $Ga_2O_3$ This is likely in part because $Ga_2O_3$ is dissolved by the electrolyte solution. $Ga_2O_3$ is predicted to form and not $Ga(OH)_3$ during cycling due to literature by the dicky research group [32]. According to Eaker et al., bases of pH larger than 10 such as the KOH solution or acids of pH less than 3, will dissolve $Ga_2O_3$ [31]. A slight secondary peak located -0.2909 V vs RHE is also present just to the left of the oxidation peak this likely due to some secondary reaction taking place. However, minimal significance was imparted to this preliminary result as copper can react with a strong basic solution and could be causing secondary reactions, despite this did show that CV testing of Ga may be achievable. Testing with a Pt wire electrode was used to obtain more unbiased data.

### *4.1.2 Platinum Electrode Results*

Finally, testing was settled with a 99.95% pure Pt wire electrode with 28-gauge diameter made by EG&G PARC Princeton Research (Catalog number RDE0021). This wire was wrapped in Teflon tape such that only the two ends were exposed so that electrical contact could be made to the potentiostat and to the Ga droplet without Pt exposed to the electrolyte and impacting the results. Test were run with liquid Ga in 6M KOH at various scan rates and then with the same configuration with the addition of powdered $Ga_2O_3$, $N_2$, sparging and varying number of cycles.

All CV plots were formatted according to the IUPAC convention with anodic current as positive upward and anodic voltage sweep to the right. Furthermore in all CV plots the current output was divided by 0.384845 $cm^2$, the cross-sectional area of the 0.7mm diameter plastic crucible which holds the Ga in contact with the Pt electrode and which is the equal to the approximate area of the exposed portion of Ga.

The first CV test was tested after only 5 cycles were scanned and showed near reversible curves however as scan rate changed, significant variability can be observed. Low scan rates (0.01 and 0.5V/s) showed almost no reduction peak however when scan rate was increased the curve showed a reversible shape until the scan rate increased to the point at which the oxidation peak diminished and reduction peak grew. These results can be observed in Fig. 13.

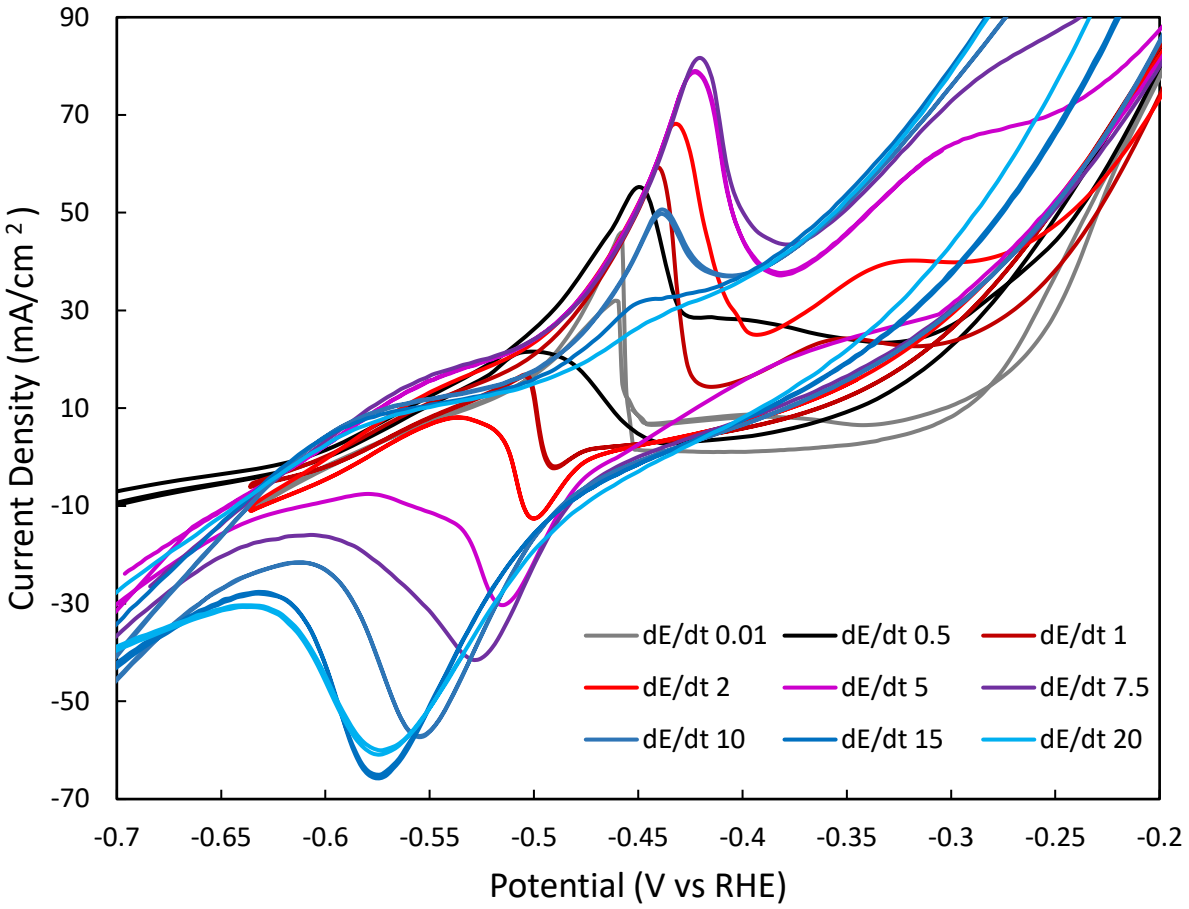


**Figure 13.** CV of Ga in KOH with graphite rod counter electrode with varying scan rates in (V/s).

Quantitative results from this test can be observed in the table 7. Numbers with (*) next to them indicate numbers approximated by sight as EC-Labs was unable to register a peak present, NA represents no apparent peak present at reducing scan.

**Table 7.** Formal reduction potentials and current ratio values associated with 5 cycles of Ga in 6M KOH.

| Scan Rate V/s | Peak Current Ratio $\lvert I_{pa}/I_{pc}\rvert$ | Formal Reduction potential vs RHE $E^{o\prime} = (E_{pa} + E_{pc})/2$ |
|---|---|---|
| **0.01** | 0.174* | -0.46 |
| **0.5** | NA | -0.467 |
| **1** | 8.866 | -0.467 |
| **2** | 3.192 | -0.467 |
| **5** | 1.777 | -0.470 |
| **7.5** | 1.569 | -0.474 |
| **10** | 0.718 | -0.496 |
| **15** | 0.308 | -0.511 |
| **20** | 0.082 | -0.508 |

*indicates values incorporating approximate values as the software could not pick up the peak.

According to the Randles–Sevcik equation $i_p = (2.69 \times 10^5)\, n^{\frac{3}{2}} A D_o^{\frac{1}{2}} C_o^* \nu^{\frac{1}{2}}$ for reversible systems, a linear relationship is present when plotting the peak anodic and cathodic current densities vs the square root of the scan rate (V/s). Often in literature peak cathodic currents are measured as negative values, however making both anodic and cathodic positive and plotting on the same diagram better demonstrates the reversibility of a system. Using this, in an ideal reversible system both lines will be collinear. Fig. 14 shows initial linearity until high scan rates are reached at which point the oxidation (blue) shows a large drop in current density.

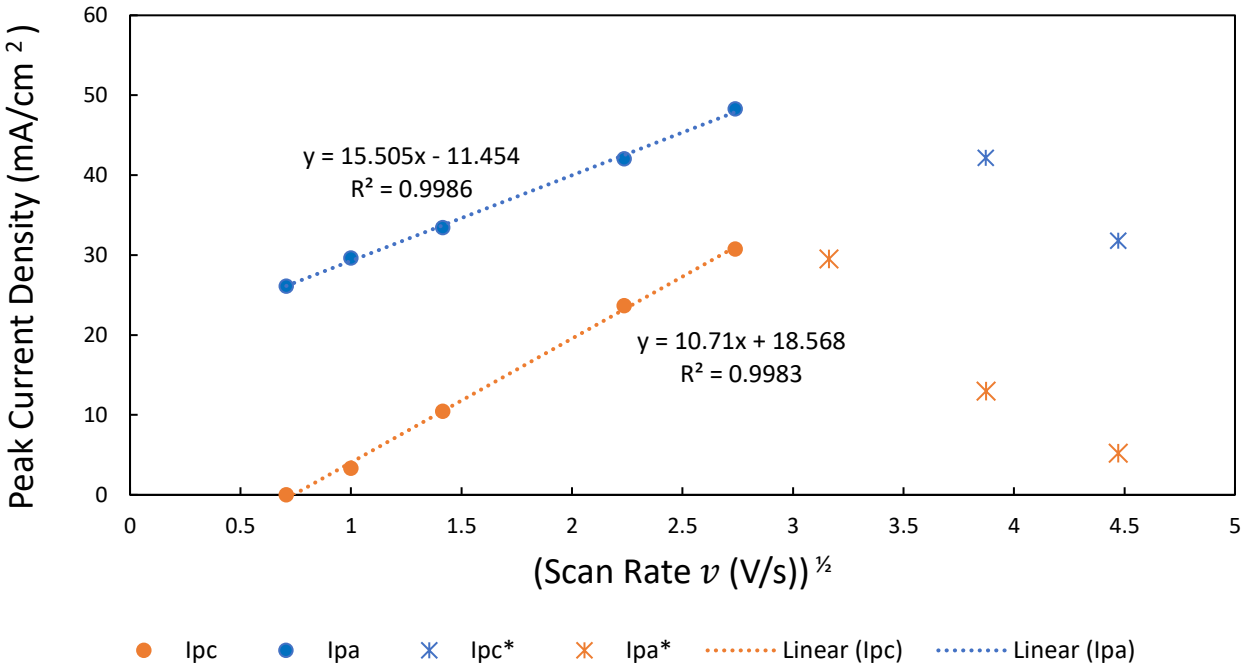


**Figure 14.** Peak anodic and cathodic current density vs the square root of the scan rate after 5 cycles, data points with stars indicate where high scan rates cause the reversible relation to drop off.

After increasing the number of cycles to 150, though there is still some variability, more symmetrical curves where obtained. Taking the 150$^{th}$ cycle results give time for stabilization to develop for charge and ion transfer. The CV results in Fig. 15 showed a more reversible curve at higher scan rates (5-20V/s), at lower scan rates the reduction peak is much smaller than the oxidation peak resulting in an uneven peak current ratio. This is likely due to the dissolution of the formed $Ga_2O_3$ and transport away from the surface of the electrode, which limits the available reactants for the reduction reactions.

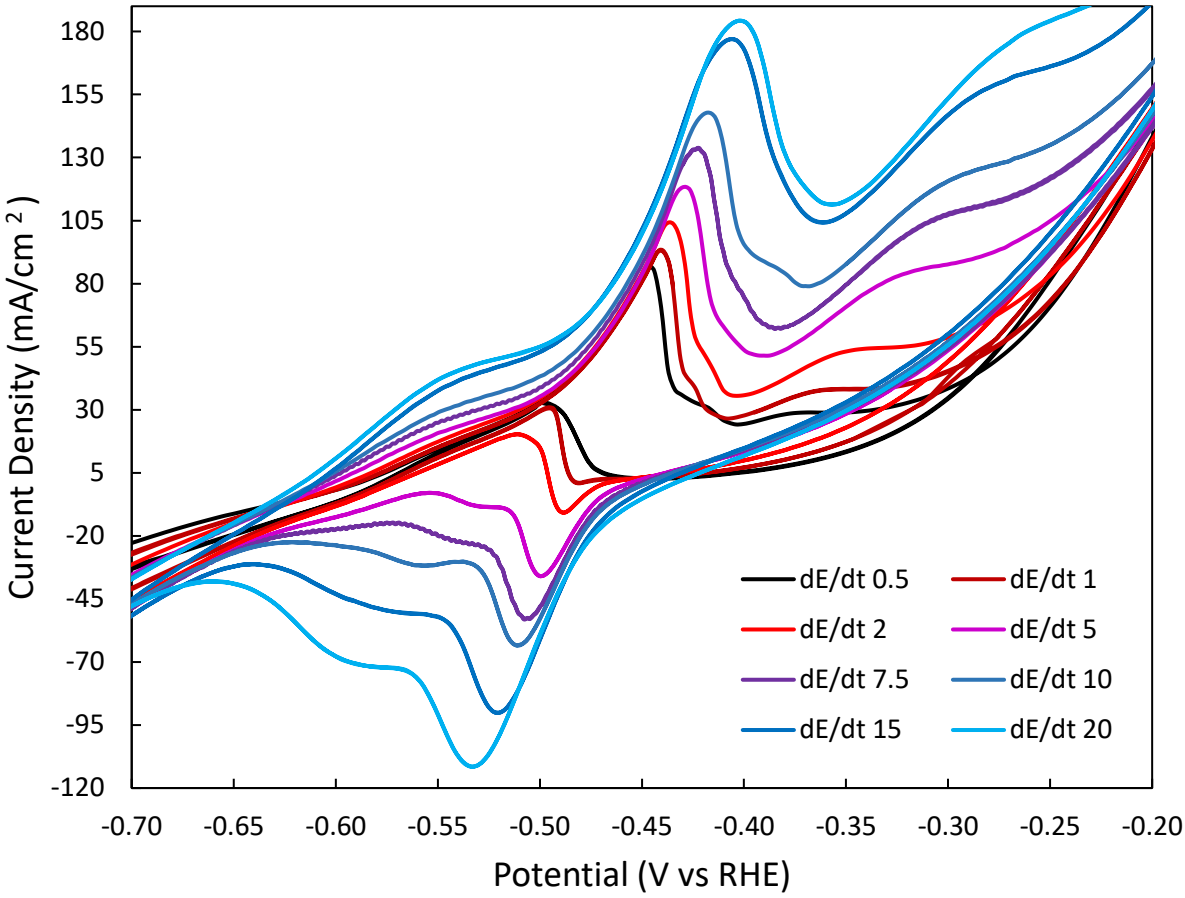


**Figure 15.** Ga in 6M KOH after 150 cycles, scan rates in terms of (V/s).

Significantly higher $R^2$ value of the linear plots shows that the linear relation between the square root of the scan rate and the peak current densities however the separation between the two lines shows that the peak current ratio is not equal to one indicating there is still some irreversibility in the current configuration.

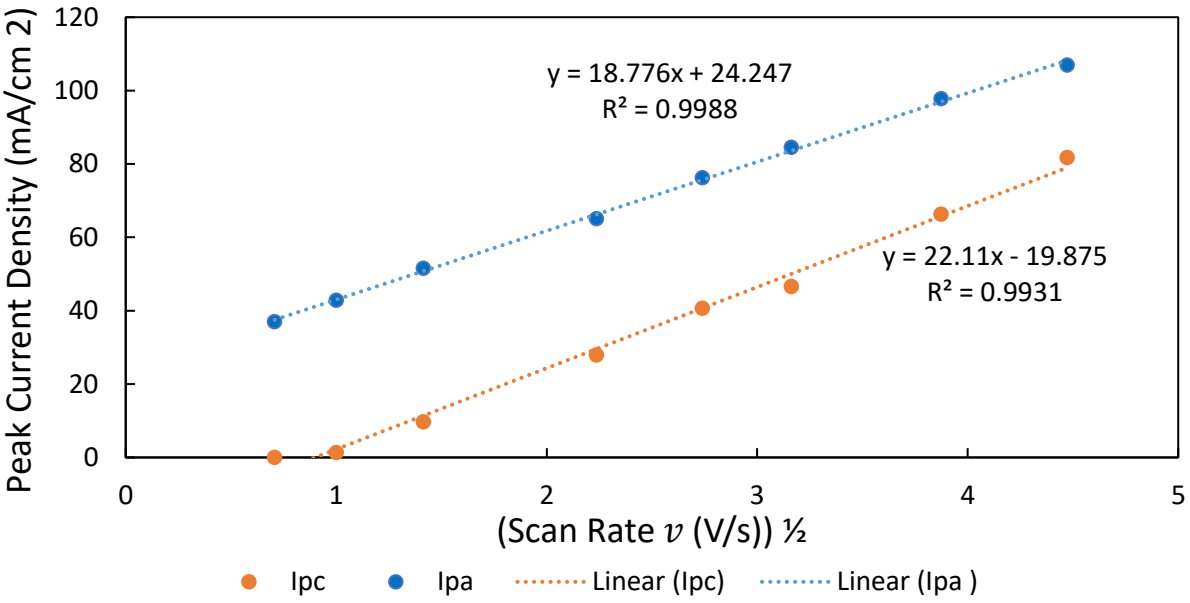


**Figure 16.** Peak anodic and cathodic current density vs the square root of the scan rate after 150 cycles.

When Observing the linear relation between peak cathodic and anodic currents, with the square root of the scan rate one, can indirectly observe the peak current ratios. The closer the two lines are, the closer to one the peak current ratio is and better reversibility.

**Table 8**. Numerical results from 150 cycles of Ga showing more stable results.

| Scan Rate V/s | Peak Current Ratio $\lvert I_{pa}/I_{pc}\rvert$ | Formal Reduction potential vs RHE $E^{o\prime} = (E_{pa} + E_{pc})/2$ |
|---|---|---|
| **0.5** | NA | -0.4575 |
| **1** | 33 | -0.461 |
| **2** | 5.289 | -0.4625 |
| **5** | 2.325 | -0.4645 |
| **7.5** | 1.874 | -0.4635 |
| **10** | 1.814 | -0.4635 |
| **15** | 1.475 | -0.464 |
| **20** | 1.307 | -0.4655 |

Using the coefficient of variation (the standard deviation divided by the mean value) to determine variability of Ep all results showed less than 2% variation of mean values with minimal fluctuation between 0.5V/s scan rates and 20V/s, further fitting the conditions of a reversible system.

Testing with the same configuration with N2 Sparging through the system for 20 minutes before and during testing showed little change in recorded potentials and current ratios. This is likely because Ga is reacting with dissolved $O_2$ and $OH^-$, in the aqueous electrolyte so even with a lack of ambient oxygen due to sparging the abundant electrolyte makes up the difference and yields minimal difference.

With the addition of unmixed $Ga_2O_3$ in solution ~1.2g in 15mL to make a super saturated suspension-solution of opaque white color. The results showed a much more symmetrical “duck shape” curve. It also showed significant improvement reaching equilibrium, reaching a more stabilized cycling after fewer cycles. Figure 17 shows the resulting symmetrical curves after only 5 cycles.

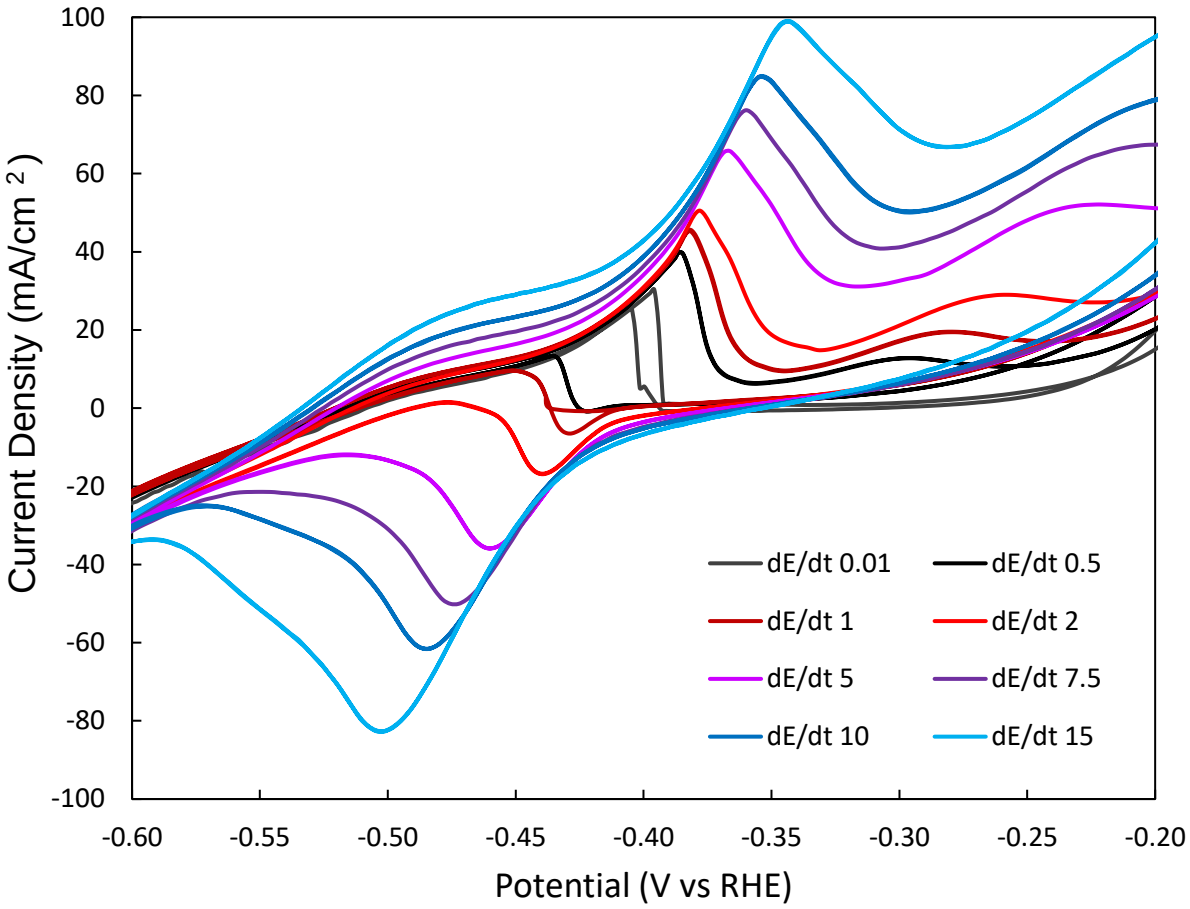


**Figure 17.** Ga + $Ga_2O_3$ suspension mixture in 6M KOH after 5 cycles, scan rates in terms of (V/s).

**Table 9.** Numerical results from 5 cycles of Ga + $Ga_2O_3$ in suspension showing more stable results.

| Scan Rate V/s | Peak Current Ratio $\lvert I_{pa}/I_{pc}\rvert$ | Formal Reduction potential vs RHE $E^{o\prime} = (E_{pa} + E_{pc})/2$ |
|---|---|---|
| **0.01** | 0.327* | -0.401 |
| **0.5** | 10.92* | -0.405 |
| **1** | 4.048 | -0.406 |
| **2** | 2.329 | -0.410 |
| **5** | 1.355 | -0.413 |
| **7.5** | 1.136 | -0.417 |
| **10** | 0.991 | -0.420 |
| **15** | 0.842 | -0.424 |
| **20** | 0.820 | -0.395 |

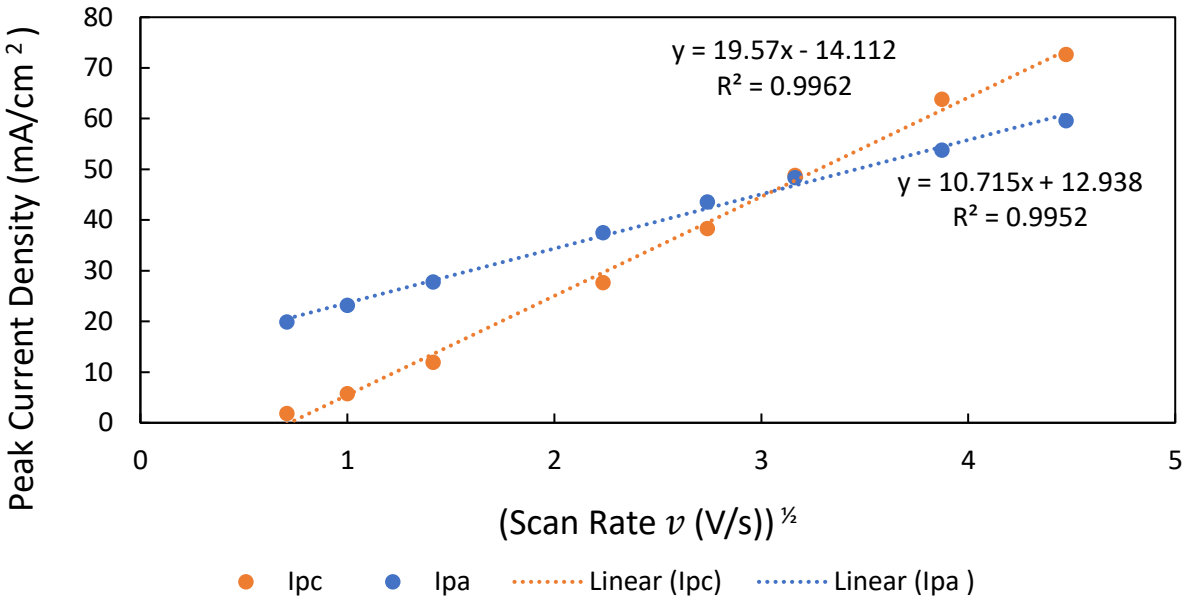


**Figure 18.** Peak anodic and cathodic current density vs the square root of the scan rate after 5 cycles + $Ga_2O_3$ suspension.

As one can see above a better linear fit across all scan rates tested, was present in the test with $Ga_2O_3$ in suspension however some variation in relative peak current densities is still present. Additionally, during some scans a secondary oxidation peak can be seen to the right of the primary peak, the matches literature findings which expect other unstable oxidation states may be forming at these peaks before dissolution. The products of these peaks are expected dissolve or dissociate away explaining why there is not a corresponding reduction peak.

Combining increased CV cycling (150cycles) to achieve stability and dissolving $Ga_2O_3$ at a 0.1M saturated concentration, gives an even higher reproducibility and symmetrical peaks as seen below.

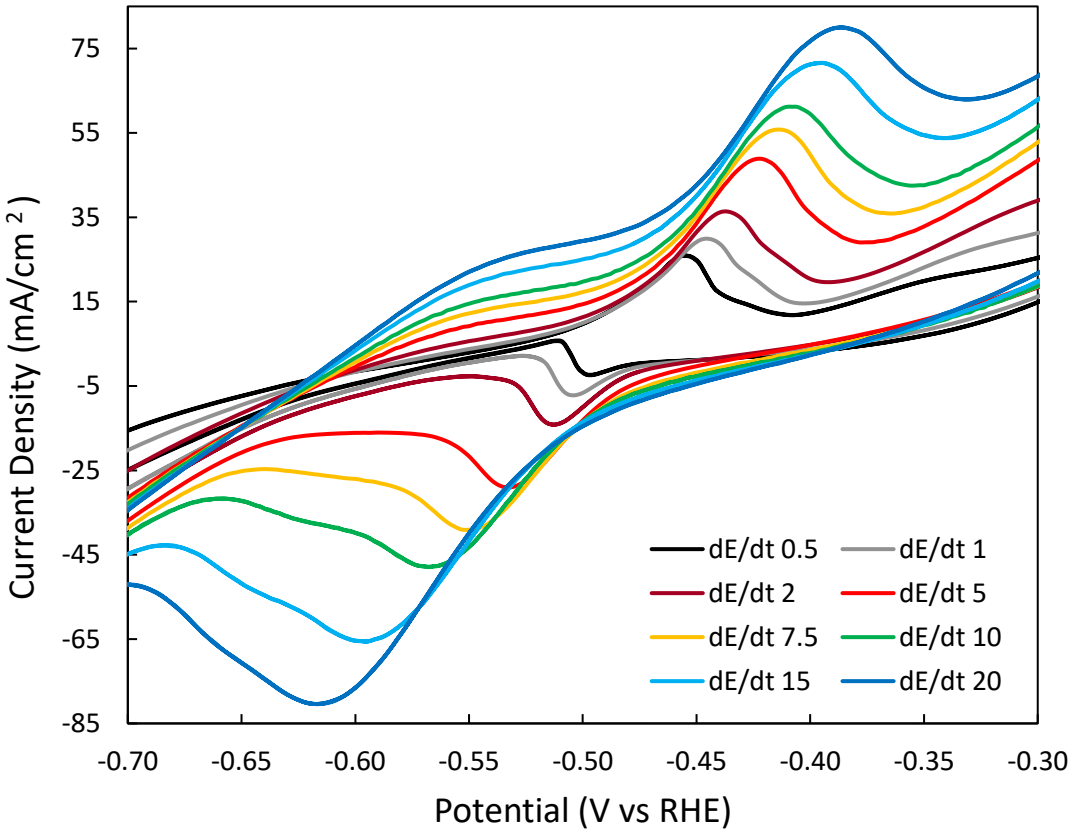


**Figure 19.** Ga + 0.1M$Ga_2O_3$ saturated dissolved mixture in 6M KOH after 150 cycles, scan rates in terms of (V/s).

With the addition of $Ga_2O_3$ one can see that a peak current ratio approaches one as the two linear plots intersect with a high $R^2$ value showing the linearity for all scan rates tested.

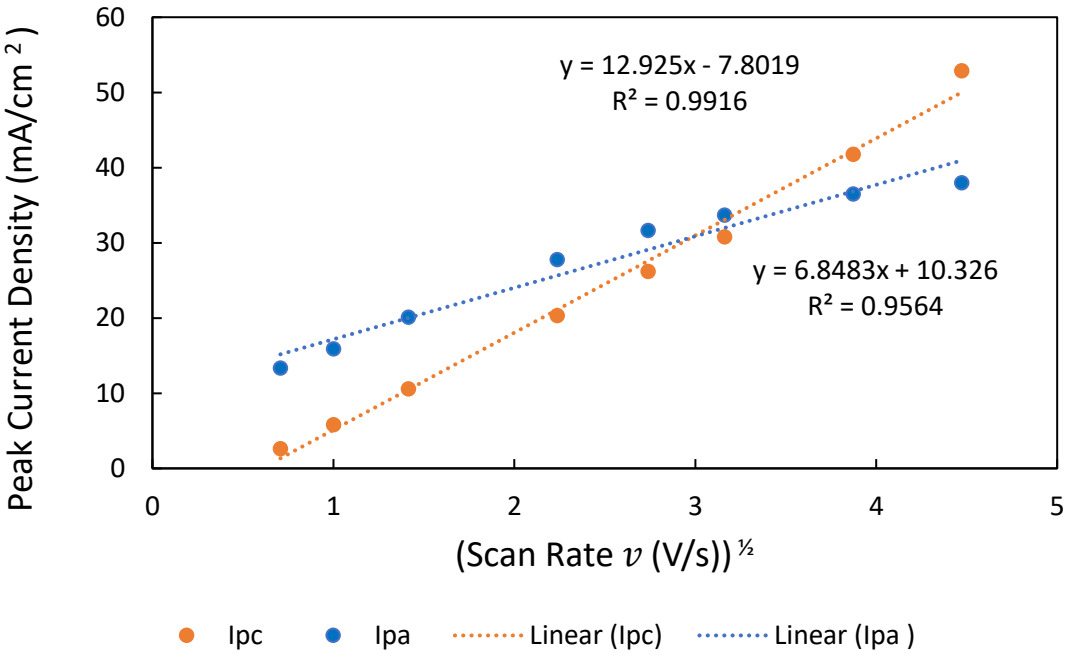


**Figure 20.** Peak anodic and cathodic current density vs the square root of the scan rate after 150 cycles + 0.1M$Ga_2O_3$ saturated dissolved mixture.

**Table 10.** Numerical results from 150 cycles of Ga +0.1M $Ga_2O_3$ dissolved in 6MKOH.

| Scan Rate V/s | Peak Current Ratio $\lvert I_{pa}/I_{pc}\rvert$ | Formal Reduction potential vs RHE $E^{o\prime} = (E_{pa} + E_{pc})/2$ |
|---|---|---|
| **0.5** | 5.127 | -0.4755 |
| **1** | 2.742268 | -0.4735 |
| **2** | 1.897178 | -0.475 |
| **5** | 1.365729 | -0.4785 |
| **7.5** | 1.207341 | -0.4815 |
| **10** | 1.093671 | -0.4865 |
| **15** | 0.873756 | -0.4955 |
| **20** | 0.718428 | -0.4995 |

To further show the increased stability and reversibility caused by the addition of dissolved $Ga_2O_3$ additional testing was sone with more data points at intermediate scan rates. The results are almost identical and show a strong linear relation though all data points collected.

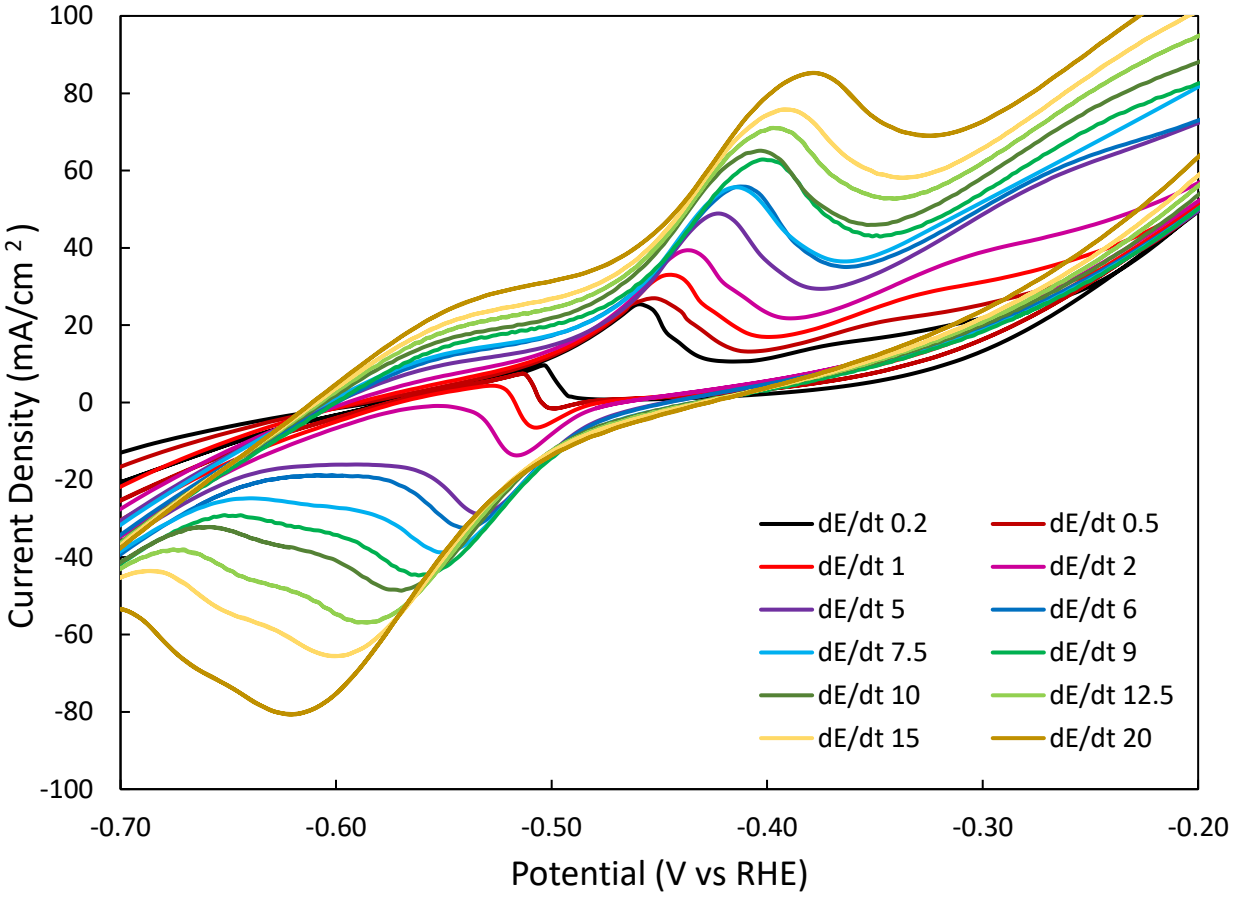


**Figure 21.** Ga + 0.1M$Ga_2O_3$ saturated dissolved mixture in 6M KOH after 150 cycles with more data points, scan rates in terms of (V/s).

The high $R^2$ values of the linear plot of this test of increased data points can be seen below.

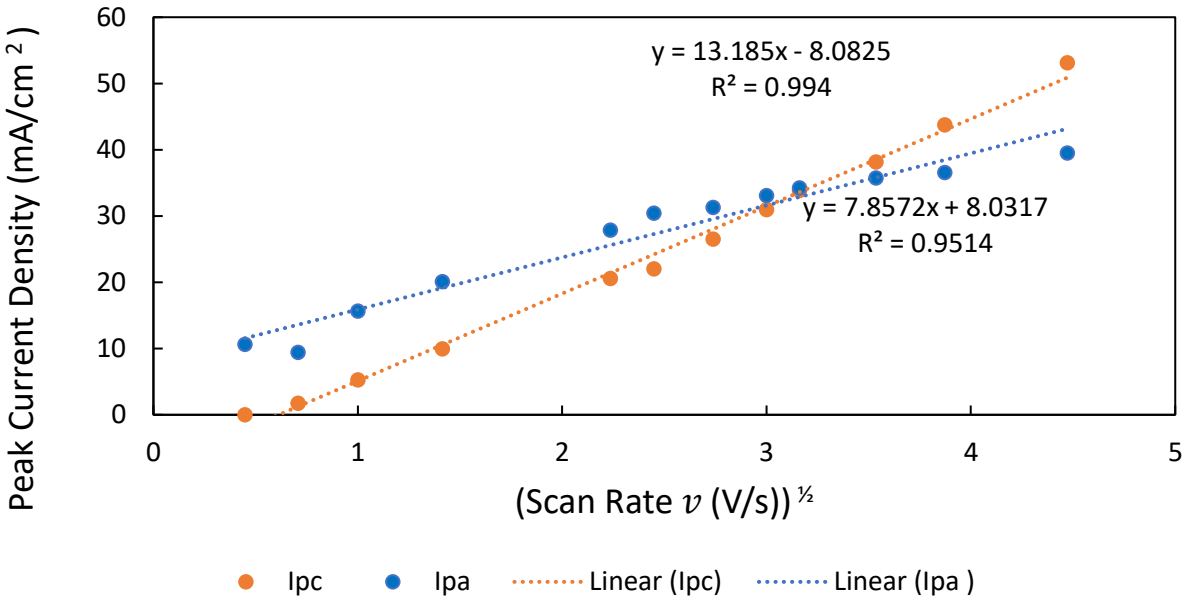


**Figure 22.** Peak anodic and cathodic current density vs the square root of the scan rate after 150 cycles with additional data points.

**Table 11**. Numerical results from second test of 150 cycles of Ga + 0.1M $Ga_2O_3$ dissolved in 6MKOH with additional scan rates.

| Scan Rate V/s | Peak Current Ratio $\lvert I_{pa}/I_{pc}\rvert$ | Formal Reduction potential vs RHE $E^{o'} = (E_{pa} + E_{pc})/2$ |
|---|---|---|
| **0.2** | NA | -0.4755 |
| **0.5** | 5.406 | -0.4805 |
| **1** | 2.982 | -0.4775 |
| **2** | 2.026 | -0.477 |
| **5** | 1.352 | -0.478 |
| **6** | 1.380 | -0.4755 |
| **7.5** | 1.180 | -0.4815 |
| **9** | 1.069 | -0.48 |
| **10** | 1.012 | -0.4865 |
| **12.5** | 0.937 | -0.4895 |
| **15** | 0.836 | -0.4925 |
| **20** | 0.743 | -0.4975 |

NA* indicates a peak current ratio which could not be obtained due to software unable to pick up a very small peak on one side.

More consistent peak current ratios near 1 can be observed from this test with dissolved $Ga_2O_3$ as can be seen in the table above.

4.1.1.1 Summary of CV results

The variability in mean peak voltage gives stability of the test as very fast reversible reactions the peak voltage will not change with scan rate. The mean value represents the calculated mean peak potential/formal reduction potential ($\mathbf{E^{o\prime}} \approx \frac{\mathbf{E_{pa}+E_{pc}}}{\mathbf{2}}$) of Ga with $H_2O$ and $OH^-$ which can be compared to prior calculations and theory. The average current ratio shows the reversibility of the system, values closer to 1 indicating higher reversibility and minimal variation shows relative stability of the redox couple. Table 11 shows these values for six different test configurations.

**Table 12**. Summary of CV formal reduction potentials, peak current ratios, and associated coefficients of variability.

| Test conditions | Ga 5 cycles | Ga 150 cycles | Ga + $N_2$ 150 cycles | Ga + $Ga_2O_3$ suspension 5 cycles | Ga+ $Ga_2O_3$ dissolved 150 Cycles | Ga+ $Ga_2O_3$ dissolved more data points 150 Cycles |
|---|---|---|---|---|---|---|
| Average formal reduction potential vs RHE | -0.480 | -0.463 | -0.481 | -0.410 | -0.483 | -0.483 |
| Coefficient of variability in mid peak voltage [%] | 3.830 | 0.507 | 1.399 | 2.152 | 1.899 | 1.423 |
| Average peak current ratio at various scan rates | 2.359 | 1.734 | 11.686 | 2.805 | 1.414 | 1.352 |
| Coefficient of variability of peak current ratio at various scan rates [%] | 129.6 | 173.4 | 217.4 | 123.2 | 49.30 | 50.20 |

The average voltages of each comes close to the -0.485 V vs RHE voltage calculated from the Pourbaix diagram. The tests on the left with dissolved $Ga_2O_3$ showed the closest average to this theoretical value. Additionally, the peak current ratios for these two tests showed average

values closest to 1 and with the least variability of all the tests indicating that the dissolved $Ga_2O_3$ increased the reversibility and stability of the redox chemistry.

The CV testing matched characteristics of a reversible electrochemical reaction. The average Ep does not vary significantly and matches theoretical thermodynamic value. The peak current ratio is equal to one for a range of different scan rates, and a linear relation between the square root of the scan rate and the peak currents exists. These reversible characteristics were most prominent in tests which contained dissolved $Ga_2O_3$ as well as Ga. However, the independent peak position of the anodic and cathodic peaks varies slightly with scan rate, $E_{pc}$ becomes more negative and $E_{pa}$ becomes more positive with increasing scan rate. This is indicative of some irreversibility according to Dr. Kayla Green, meaning some irreversibility is present [29]. Additionally, $E_{pa} - E_{pc} = 2.30 \frac{RT}{nF}$ matches the results present at low scan rates however at higher scan rates Epa-Epc> $2.3 \frac{RT}{nF}$ which is consistent with a quasi-reversible system [29]. This can also be due to resistance in the electrolyte solution and large separation between electrodes and experimentally rarely fits the data.

Figure 23 shows the observed formal reduction potential (-0.47v vs RHE) is compared with the reduction potential calculated by the past MQPs of $Ga_2O_3$ (-0.450v vs RHE) and $Ga(OH)_3$ (-0.369v vs RHE) production.

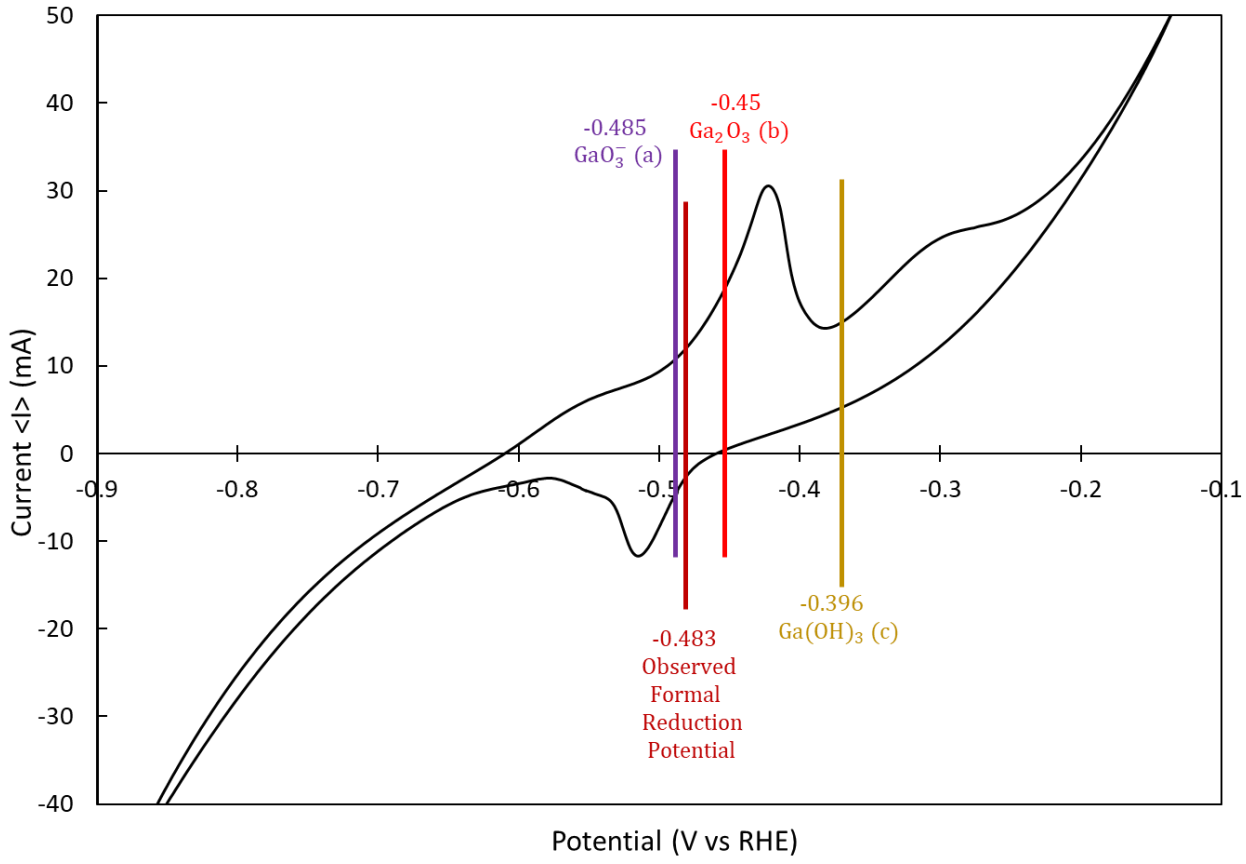


**Figure 23.** Voltammogram with calculated and observed voltages marked, Ga in 6M KOH with scan rate of 5V/s.

**a)** corresponds to the calculated Pourbaix potential for $GaO_3^{3-}$ formation, **b)** calculated voltage of $Ga_2O_3$ formation from the past MQPs and **c)** the voltage corresponding with $Ga(OH)_3$ calculated by past MQPs. Often in application the calculated (ideal) voltage is slightly off the measured because of imbalanced overpotentials, equipment calibration and internal resistance of the system. As a result, the above shows a high likelihood that the reaction observed is indeed $GaO_3^{3-}$ which is the dissolved version of $Ga_2O_3$ is being formed. Because the voltage calculated from the Pourbaix reaction equations considers the specific pH of the test it is more applicable to

the CV test configuration compared to the value calculated by the past MQPs which assumed standard conditions of pH 7.

#### 4.1.2.1 Testing other pH electrolytes

Tests were also run using HNO3 and KBr to evaluate effects of an acid and neutral electrolyte on the systems rechargeability. However, the resulting data was unreadable. Tests with 6M KBr ran into issues. Whenever a voltage was applied KBr crystals began forming on the working and counter electrode surfaces as well as on the surface of the liquid. This made it difficult to obtain clear readings due to inability of ionic diffusion and inconsistent electrical connection during testing. Furthermore, at a neutral pH $Ga_2O_3$ is not dissolved spontaneously by the electrolyte, so a thin layer could be seen on the surface as the Ga droplet tested did not have a pristine shiny and uniform sphere like shape before voltage was applied. This made it clear reduction was occurring once a voltage was applied because the slight non-reflective $Ga_2O_3$ and odd shape was replaced by reflective Ga droplet with uniform curvature once a voltage was applied to the system. Additionally, the wetting properties of Ga with Pt at this pH are different relative to in the KOH solution. Initial contact could be made before test was started however once the Ga was reduced and test was started the Ga develops an aversion to the Pt causing inconsistent electrical connection and unreadable results.

Since Ga oxidation to $Ga_2O_3$ is not a proton-dependent reaction, the standard potential is not changed as the pH of the surrounding system is altered. However, as pH is lowered from basic to acidic in an aqueous electrolyte, the propensity of other reactions to occur increases. As the pH decreases hydrogen evolution becomes progressively more thermodynamically favorable. In a basic solution the reduction potential of Ga is~-0.4 V vs RHE meaning only -0.4 V below the reduction potential necessary for hydrogen evolution to occur. At this voltage there is still a slight

over potential as well as kinetic limitations which make the Ga to $Ga_2O_3$ preferable and less obscured by $H_2$ evolution. However, when the pH is decreased in a neutral or acidic solution the voltage applied in relative to the hydrogen reduction voltage RHE increases significantly, causing the hydrogen evolution to be a more thermodynamically favorable process. Because resulting currents and side reactions increase as the favorability of this reaction grows, the clarity CV data is lost with lower pH.

The graph below (Fig. 24) shows the irregularity of results with HNO3. The irregularity is due to poor wetting and electrical connection between the Ga and Pt electrode due to changed surface characteristics at high pH. Noting the vertical axis, much higher currents are present relative to the KOH tests which did not exceed ~60mA further indicating that electrolysis is thermodynamically more favored in this configuration.

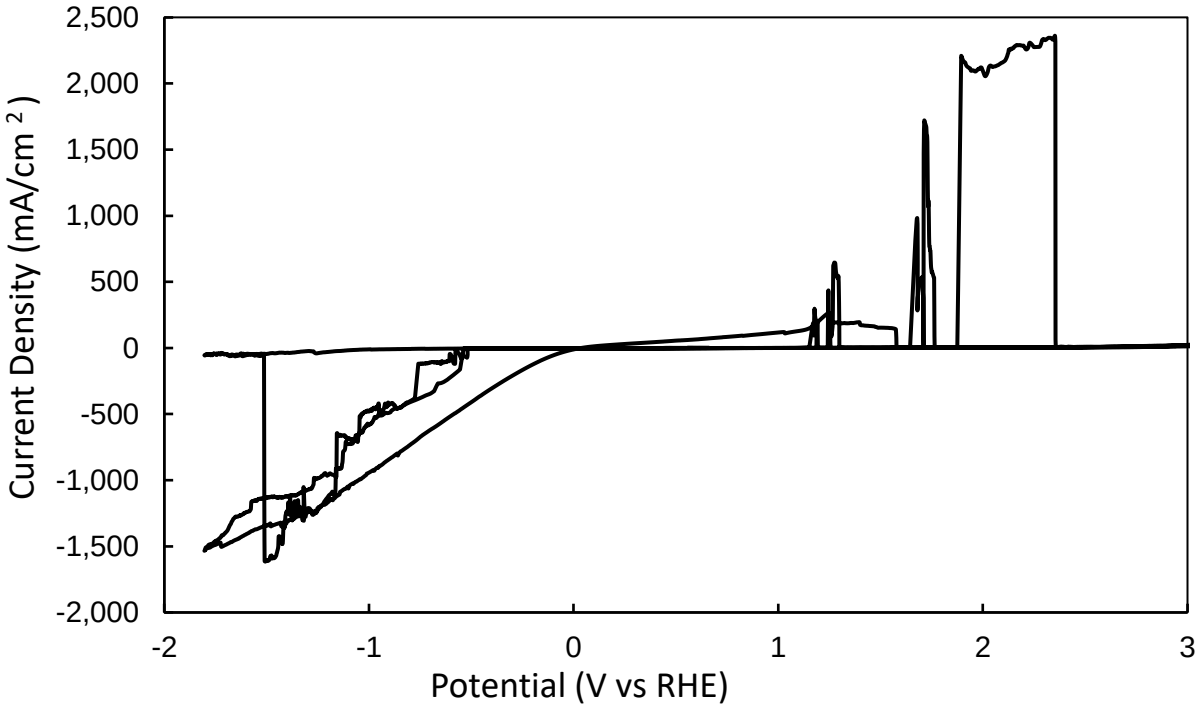


**Figure 24.** Unreadable CV results of Ga in HNO3 at a scan rate of 0.5 (V/s) due to different surface characteristics and poor wetting/electrical contact between Pt and Ga at this high pH.

Another set of issues arose when the reference electrode used was dried out after not being stored correctly. This issue resulted in an irregular connection between reference electrode and electrolyte solution that caused the system to have a slight capacitive response. Where charge was built up and discharged in bursts. This spiking resulted in irregular data with jumps in current making it unreadable, these could be observed at the working electrode as short bursts of electrolysis (bubbles). Once it was discovered that the reference electrode was dried tests were resumed with another working reference electrode, which once again matched initial tests.

A few details of note can be extracted from the CV testing at this point. First, the tests resulted showed a central peak voltage ($E_p$) near that of the net anode reaction expected of $Ga_2O_3$ formation calculated by past MQPs. Next the tests confirmed that hydrogen evolution is an issue with the current electrolyte configuration. Because the redox voltage of Ga is less than zero vs RHE hydrogen evolution can take place. This is less an issue with discharge as the over potential typically causes a lower discharge current, however for this battery chemistry to be rechargeable it will need to charge at a higher voltage so that the over potential of Ga is overcome, and effective charging may be successful. A higher voltage during recharging will cause hydrogen evolution to be an even larger issue causing degradation of aqueous electrolytes. And lastly, at certain scan rates the peak to peak ratio of this reaction is 1 indicating that this could be an effective rechargeable battery chemistry however this may be altered with the addition of an organic solvent electrolyte and the removal of water in the chemistry.

**4.2 Electrodeposition Charge Test**

Previous projects were unable to show that Ga to $Ga_2O_3$ is reversible into Ga by charging however Fig. 25 show that this reaction is reversible and possible. $Ga_2O_3$ was mixed

in 6M KOH to form a saturated suspension solution (before full dissolution is attained). The Pt electrode and graphite rod used for CV testing were put into the solution and a constant current of 1mA was applied between the two for 1hr, with negative connection to Pt and positive to graphite. In Fig. 25 the left image shows the Pt electrode prior to testing and the right after Ga was electroplated on to the electrode. As the photos were taken over a 5-minute period the pure mirror like Ga began oxidizing forming the mottled surface observable near the top of the deposited Ga.

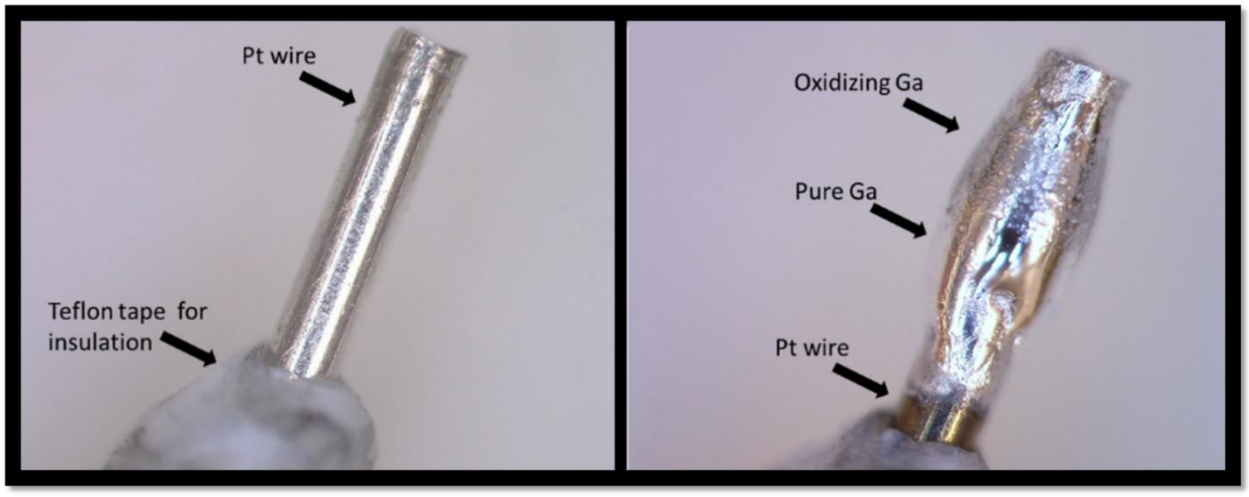


**Figure 25.** Ga electroplated from oxide solution on to Pt electrode.

Using the diameter of the Pt wire as the known scale (28-gauge = 0.32mm) the image on the right was processed in ImageJ to calculate the perpendicular area of the Ga deposited on one side of the electrode $0.091\text{mm}^2$. Approximating the centroid of this area relative to the axis of the electrode ($R_{\text{Centroid}} = 0.171\text{mm}$) the theorem of Pappus was employed to determine the volume of the deposited Ga on the electrode, $0.1031\text{mm}^3$. This volume was converted to the number of moles of Ga plated $8.734\mu\text{molGa}$. Used in conjunction with the charge time and current transferred the overall coulombic efficiency of the electrodeposition was calculated.

The number of electrons transferred when charging at 1mA for 1hr was found and compared to the amount of Ga plated.

$$1\text{mA} \times 1\text{hr} = \frac{1\text{mcoulomb}}{1\text{sec}} \times 1\text{hr} \times \frac{3600\text{sec}}{1\text{hr}} \times \frac{1\text{coulomb}}{10^3\text{mcoulomb}} \times \frac{0.625*10^{19}\text{e}^-}{1\text{coulomb}} \times \frac{1\text{mol e}-}{6.02210^{23}\text{e}-} = 37.36\mu\text{mol e}^-$$

Assuming a 3 electron transfer necessary for $Ga_2O_3$ reduction.

$$8.734\mu\text{molGa} \times \frac{3\text{e}^-}{1\text{Ga}} = 26.202\mu\text{mol e}^- \text{ used for reduction.}$$

Which gives a culombic efficency of $\frac{26.202\mu\text{mol e}^-}{37.36\mu\text{mol e}^-}$ = ~ 70% meaning ~30% of the transferred electrons are being lost to other reactions, likely hydrogen evolution reaction (HER) due to slight noticible bubling at the negitive electrode and the induced potential range. This test was reproduced on both the Battery Metric Analyizer as well as on the Potentiostat using the GCPL2 (galvanostatic cycling with potential limitation 2) program which allows a counter electrod to be used to further investigate the reactions present at the two electrodes while charging. Using the potentiostate the voltage difference between electrodes was ~2.5 V with the value at the reducing electrode of ~-1.75 V vs SHE. This fits with the solid Ga portion of the Pourbaix diagram and taking into account a slight over potential of 0.4 V commonly required for charging reactions matched the expected requirment for charging.

### 4.3 Battery Analyzer Results

Over the course of running the different configurations of the cell, the Swagelok configuration that seemed to be the most efficient was where the crucible contained liquid metal Ga with Ga (III) trioxide in 6M KOH wetted alternating Zr cloth, polypropylene separators with the cloth closest the electrodes, Ga anode and oxygen cathode, and polypropylene in the middle as modeled below.

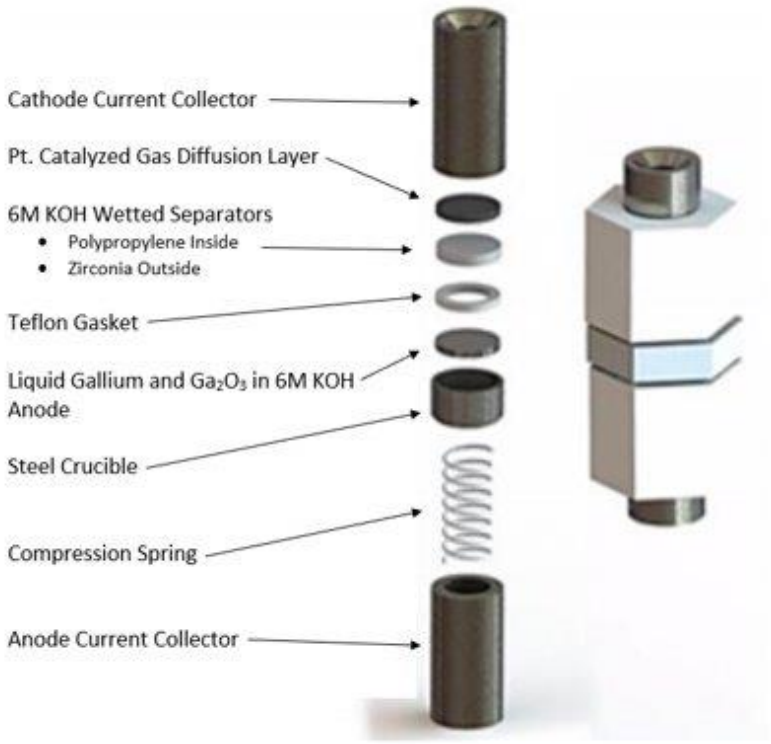


**Figure 26.** Modified cell configuration adapted from Howard, et al. [7].

This configuration allowed for electron transfer of the Ga anode while restricting leakage of the $Ga_2O_3$ in KOH through the separators. It also allowed the cell to have steady discharge voltages and times as well as attaining rechargeability. The experiments using the Swagelok cell testing were conducted using a BA500WIN Battery Metric. Different tests were conducted to test the feasibility of this battery and its configuration and included charge/discharge profiles with multiple cycles, alternating and varying separator type and quantity in a vacuum, discharge with nitrogen gas sparging and polarization curves for comparison with current liquid metal-air and metal-air batteries such as Zn-air and liquid Tin-air. Images of the set up and post experiment cells can be found in Appendix C.

### *4.3.1 Polarization and Discharge Kinetics*

The procedures we used for setting up the Swagelok cell for the liquid Ga-air battery were based on the conditions and programs conducted in the previous year's MQPs. Despite running the cell under same conditions and using the same cell, we found that most of our tests were not comparable to that of the previous years. Throughout our experimentation, we found that there was a difficulty in recreating the discharge times achieved in previous years and the program would often have a lot of "noise". Below are a few of the discharge curves that we found when trying to reproduce the results from the previous MQPs.

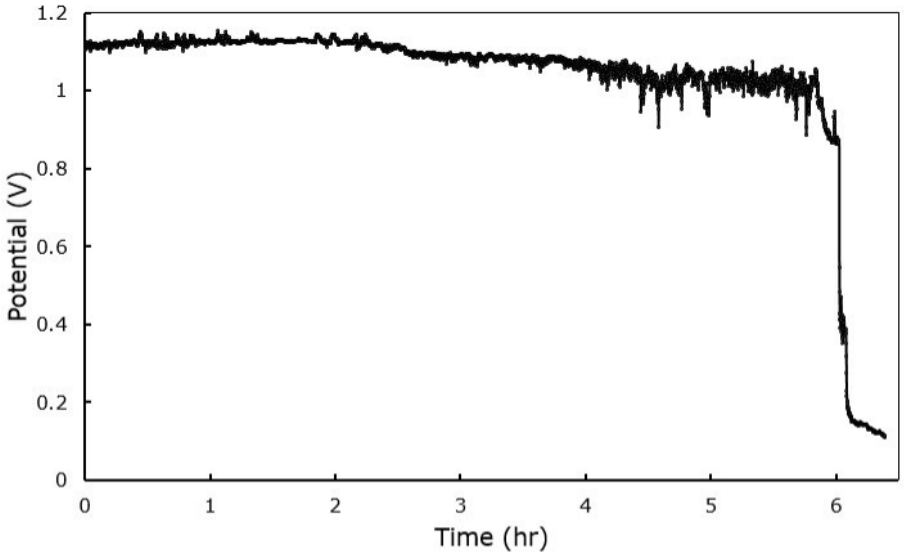


**Figure 27.** Ga-air battery discharge curve with two separator system at ~50 °C and 7.99 mA/cm$^2$

In the discharge curve above, we had a resulting discharge time of just over 6 hours and an overall electric charge of 308 mAh making it one of the best results we got in terms of reproducibility with the previous MQPs. However, we found that some tests would result in lesser discharge times through a short circuit in the cell. Despite this being against our intended outcome, we discovered different possible reasons that the cell might not be working as intended. We believed these setbacks to be a result of Ga seeping through the pores in the Zr cloth as well as the evaporation of the Potassium Hydroxide (KOH) electrolyte in the separators. This was concluded

as a result of the graphs sporadically changing voltage as with Figure 33, or with the extremely depleted discharge time and strange shape as in Figure 34.

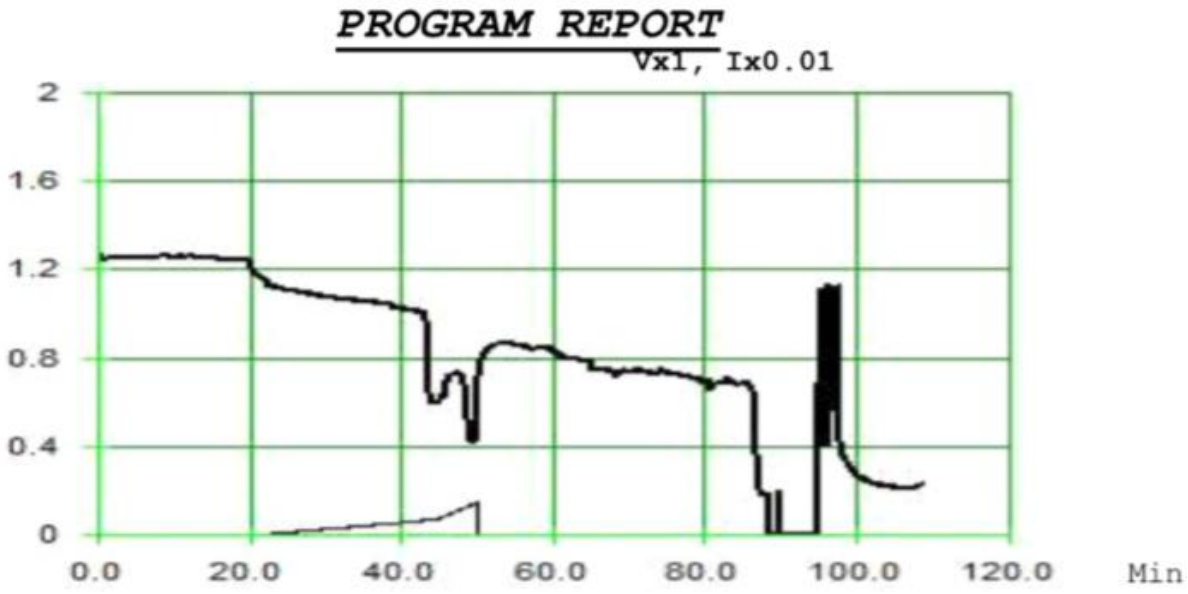


**Figure 28.** Ga-air battery discharge curve with Ga seepage.

The graph above was the result of an experiment in which we found that the Ga partially leaked through both the separators as well as the gas diffusion layer then continued to exit through the bottom of the cell. We believe the declining voltage of the graph was due to the gradual introduction Ga through the separators. Once the Ga started to seep through, we believe that the cell began to short circuit and as that occurred, the voltage approached zero and sporadically jumped before finishing. In the experiment below, the battery ran for about 13 hours before short circuiting. We believe this is perhaps due to the electrolyte KOH evaporating or electrolyzing

which would restrict ion transfer and impede the discharge of the battery.

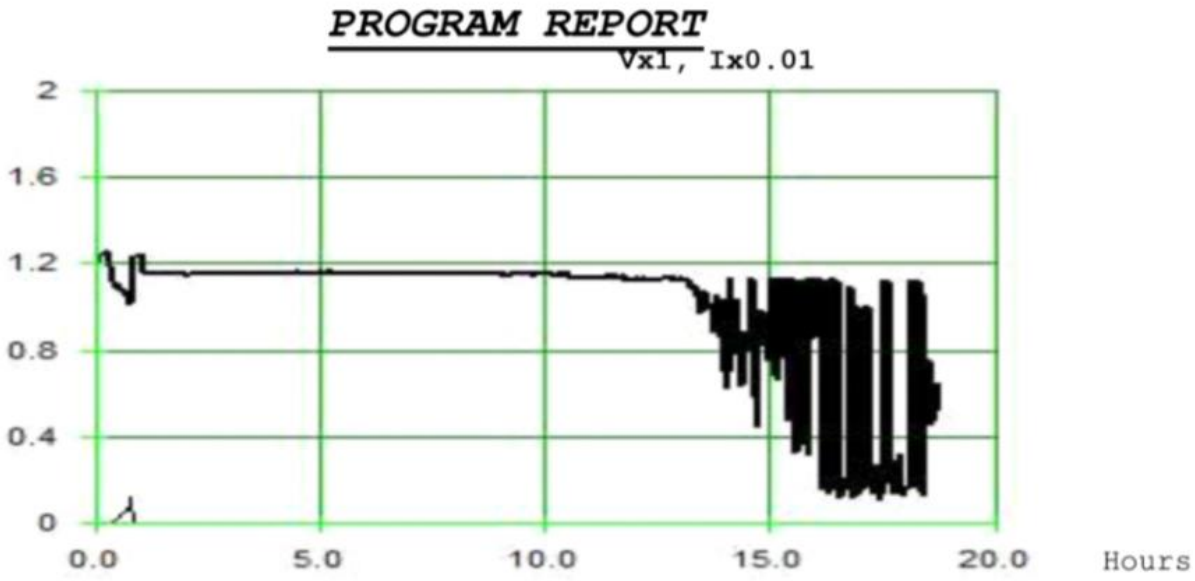


**Figure 29.** Longest discharge of Ga-air battery that short circuited

Despite having difficulty in trying to reproduce the data from previous years, we used the shortcomings of these runs to create a new modified cell which may overcome some the obstacles experienced. To eliminate the tendency of the Ga and KOH electrolyte to seep through the Zr cloth separators, we found that using polypropylene separators in conjunction with the Zr cloth would restrict seepage while maintaining the electrochemical character of the cell and prevent short circuiting. Another idea was to use Ga (III) trioxide in 6M KOH electrolyte to prevent electrolysis of the electrolyte. This theory was proven by two Russian researchers, Kochegarov and Lomakin, in 1964 when they conducted experiments and found that during Ga electroplating, hydrogen evolution was mitigated through utilizing high gallate concentrations (Yonghwa Chung and Chi-Woo Lee). Given these modifications, we ran the discharge programs again and plotted the results against a commercial Zn-air battery.

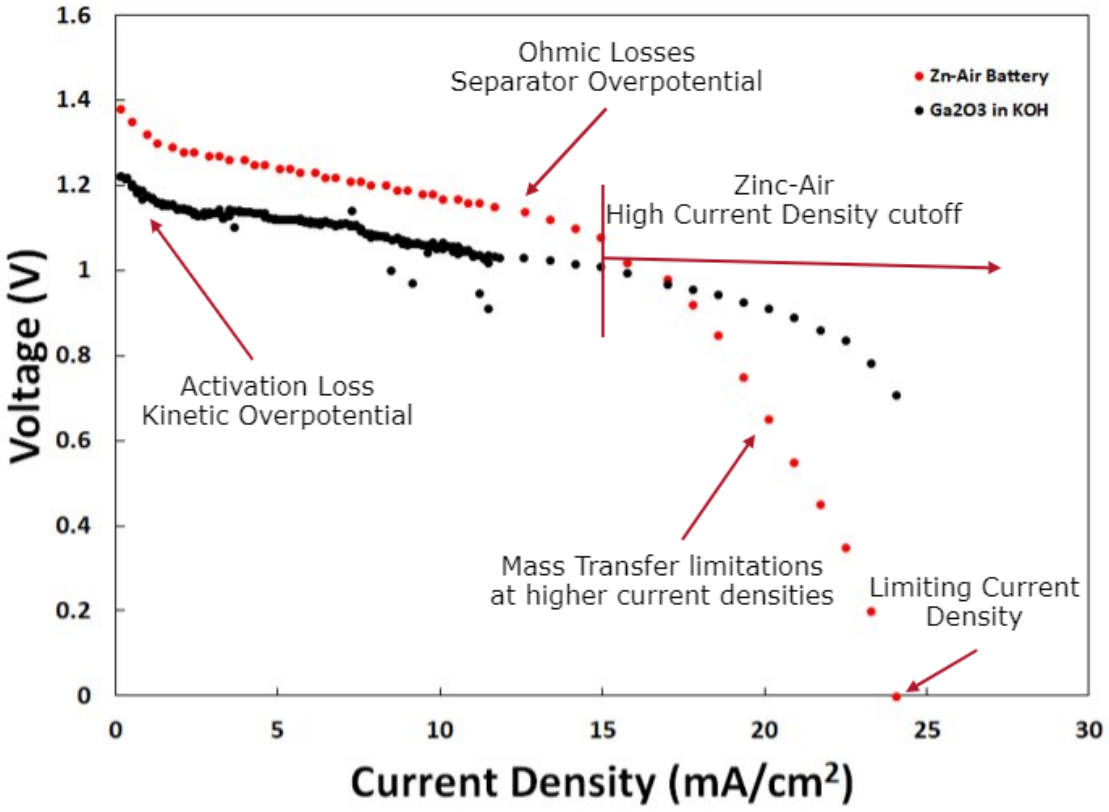


**Figure 30**. Polarization curves of a Zn-air battery compared to Ga-air battery with dissolved $Ga_2O_3$ in KOH with varying separators with Zr cloth nearest the electrodes and polypropylene in between

In the Zn-air battery, the anode is comprised of a Zn powder mixed with gelled KOH electrolyte, causing the electrochemical area to be far greater than the geometric area. Despite this having the effect of a decreased material usage, it has an adverse effect on the potential relationship with current density compared to the modified Ga-air cell. Due to the smaller area of reaction in the Ga cell, higher current densities were achieved with minimal loss of potential. As can be seen in the polarization curve, despite the commercial Zn-air having a higher open circuit voltage compared to that of the Ga-air battery, the Ga-air battery could attain higher current densities while relatively maintaining its voltage while the Zn-air had lost its potential to mass transport and activation losses well beforehand.

### *4.3.2 Charge/Discharge Cycles*

From the results of the CV analysis, we determined that the cell had the capacity for rechargeability and had the potential to be used as a secondary battery. With that in mind, we decided to run discharge/charge cycle runs to test how running the cell through numerous cycles would affect battery performance and if there would be any loss in potential from the repetition. For the charge / discharge runs we conducted, we compared the original cell to that of the modified cell. In both cases, the cell was able to charge and discharge for the entirety of the programmed step function and remained at a steady voltage. Both cells had similar results with the major difference being their discharge voltages with the original cell's potential began decreasing towards the end of its discharge while the modified cell held constant. The program was then written for an initial discharge at 0.5 mA current and a voltage cutoff of 0.3 V with subsequent charge/discharge cycles at the same current and an hour in duration. The following graphs are the results.

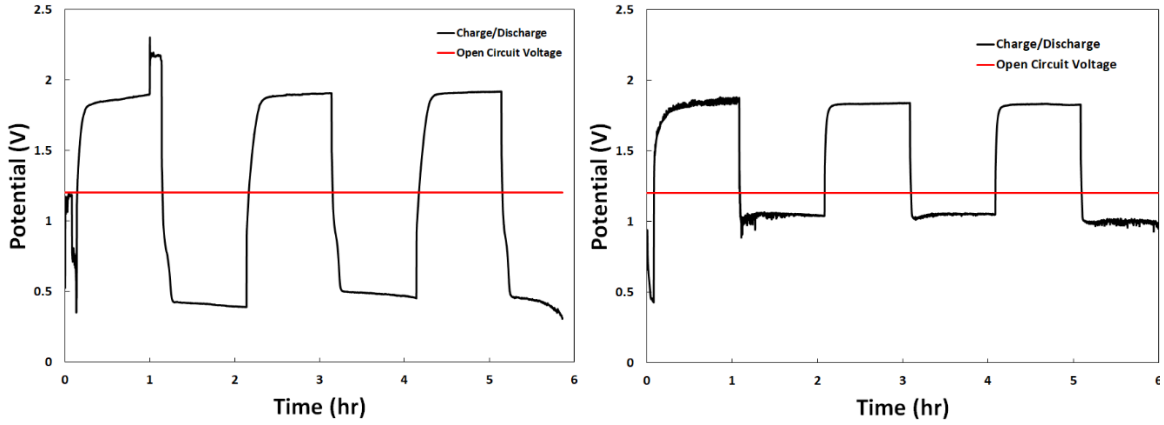


**Figure 31.** Charge/discharge cycles at 0.5 mA current. **Left.** Original cell **Right.** Presence of $Ga_2O_3$ in KOH.

As is shown, both cells had the capacity of charging and discharging, however the cell with presence of $Ga_2O_3$ in KOH had a higher voltage of discharge compared to that of the original cell, most likely due to the $Ga_2O_3$ presence mitigating hydrogen evolution and favoring reduction of

$Ga_2O_3$. Also, the original cell appears to have a slowly declining discharge potential, possibly due to seeping Ga. This further showed improvement with adding $Ga_2O_3$ to the cell.

### *4.3.3 Restricted Air Flow with Varying Separators and Nitrogen Sparging*

To test the effect of increasing quantity of separators in a cell with restricted air flow, we set up the cell in such a way that there was as little air flow into the cathode of the cell and tests were run with increasing quantity of Zr cloth separators. Set up can be seen in Appendix C. As a result, we found that, without any oxygen to react, the voltage and discharge times were limited but increased with increasing number of separators. As seen in the figures below, with a cell using one Zr cloth separator averaged a discharge voltage of 0.7 V and lasted about 6 minutes while with two separators, the discharge time increased to around 25 minutes and further to 35 minutes with three separators. Also, as the number of separators increased and the discharge time increased, the potential would start to decline, decreasing the average discharge potential and also shows that maintaining a discharge for the original cell may be adversely affected by its current setup.

Beyond testing the impacts of additional separator layers on effect on discharge time, we tested the effect of $N_2$ sparging through the cell to determine the dependence of the reaction on oxygen as well as how the cell would react with an abundance of Nitrogen as present in ambient air. To test oxygen's role in the reaction, we conducted an experiment where we sparged Nitrogen gas through the cell and measured the discharge. From the resulting graph, we found that, although the cell was still able to discharge despite the absence of oxygen contributing to the reaction, the battery was unable to discharge as well and long as what was found with oxygen being involved in the reaction. As a result, the potential of the cell was greatly diminished and was sporadic towards the end (Fig. 32), indicating there is a dependence on ambient oxygen in the battery.

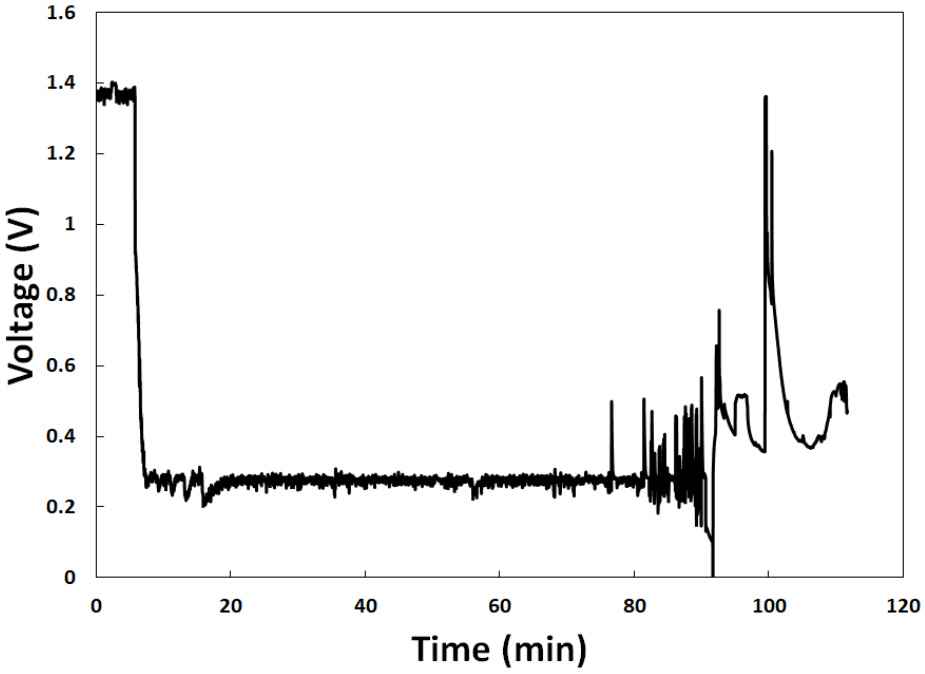


**Figure 32**. Nitrogen gas sparging discharge curve.

### *4.3.4 Calculations Evaluating the Quantity of KOH in Battery Tests*

Calculations were made to determine the quantity of KOH contained in the two separators as well as the quantity of electrons being transferred during discharge. This was done to compare the quantity of electrons being transferred with the amount of KOH available for ion transportation and charge balance to evaluate if KOH is a limiting factor in the battery reaction. cloth separators were weighed before and after soaking for ~20 minutes, afterwards the average change in weight was calculated which was later used for calculations. Below the table 13 of results associated calculations can be seen.

**Table 13**. Mass of dry and wet separators.

| | Mass of Dry Zirconia (g) | Mass of Zirconia soaked in 6M KOH (g) | Difference in Mass (g) |
|---|---|---|---|
| Separator 1 | 0.0320 | 0.1048 | 0.0728 |
| Separator 2 | 0.0314 | 0.0987 | 0.0673 |
| Separator 3 | 0.0316 | 0.1113 | 0.0797 |

An average difference in mass of 0.0733g was calculated. According to engineering toolbox the density of a 6M solution of KOH is ~1.25 g/cm$^3$ which can provide the quantity of KOH per separator.

$$0.0733\text{g} \times \frac{1\ \text{cm}^3}{1.25\text{g}} \times \frac{0.001\text{L}}{1\text{cm}^3} \times \frac{6\ \text{mol}}{1\text{L}} \approx 0.00035184\ \text{mols of KOH per separator}$$

Therefore, the average amount of KOH per test cell using two separators is 0.00070368 mols, which can be used for further calculations and assessment of the depth of battery discharge in the subsequent section.

### *4.3.5 Calculations to Evaluate the Quantity of Ga Reacting in Prototype cell*

When saving results from the battery analyzer the capacity for each given step is compiled. To find the total discharge of each test the sum of each step is taken. This would be equivalent to integrating the area under the discharge-time curve to obtain the total capacity of the test in mAh.

$$\text{Total capacity} = \sum \text{x[mAh]}_\text{i}$$

For example, discharge test 2 gave a total discharge capacity of 6.9836mAh, a low value relative to the optimized Zn-air button batteries which capacities of 150-300mAh commercially. However, this value is till promising in rudimentary prototype for proof of concept.

$$6.9836\text{mAh} \times \frac{1\text{mAh}}{1000\text{mAh}} \times \frac{1\text{mol e}^-}{26.8\text{Ah}} \times \frac{1\text{mol Ga}}{3\text{mol e}^-} = 0.0000868069\ (\text{mols of Ga reacted})$$

$$0.0000868069\ \text{mol Ga} \times 69.723 \frac{\text{g}}{\text{mol Ga}} = 0.006056188\ (\text{grams of Ga reacted})$$

As 1.2g of Ga is loaded into the Swagelok cell during each test, the relative proportion of reacted Ga can be calculated.

$$\frac{1.2\text{g} - 0.006056188\text{g}}{1.2\text{g}} \times 100 = 99.4953\%\ \text{Ga unreacted in crucible}$$

From the separator calculations one can determine the amount of KOH in the cell and there for the extent at which the reaction could progress.

$$\frac{1.2\ \text{g Ga availible}}{69.723\ \frac{\text{g Ga}}{\text{mol Ga}}} = 0.017211\ (\text{mol Ga availible per test})$$

Using this value, we calculated the ratio of Ga which could react if all the electrolyte was consumed.

$$\frac{0.017211\ \text{Ga per test} - \frac{0.00070368\ \text{mol OH}^{-}\ \text{per 2 seporators}}{3\ \text{e}^{-}\ \text{needed per Ga reaction}}}{0.017211\ \text{Ga per test}} = 98.6371\%\ \text{Ga unreacted}$$

These calculations show how little Ga is reacting in these tests. Once limiting factors are evaluated and tests are adjusted accordingly the discharge capability of this type of battery could be significantly improved. Currently as in work of past MQPs, water evaporation in the electrolyte and good sealing between battery layers are likely key limiting steps.

### *4.3.6 Reaction Depth Calculations*

Using the results of the above calculations one can calculate the theoretical thickness of a forming $Ga_2O_3$ film to determine if the $Ga_2O_3$ is only reacting at a surface mono layer or farther into the Ga. Sample calculations which can be seen in Appendix D, result in 28940 layers of $Ga_2O_3$ deposited on the droplet assuming uniform distribution over a spherical Ga droplet and ideal dissolution conditions.

Though just a rough calculation this suggests that more Ga is oxidizing than one would likely see if only a monolayer was forming. However, a substantial layer was not optically

observed so indicating that a passivating layer is unlikely the cause of cell death though it cannot be excluded at this point. One notable detail is that the quantity of Ga reacted is of the same magnitude as that of the quantity soluble in the present amount of electrolyte. The indicates that that the quantity of electrolyte may be limiting the cell to some extent.

# 5.0 Conclusions and Future Work

## 5.1 Conclusion

This project took a prototype battery cell found in previous MQPs and studied the fundamental reactions taking place through CV to better determine and optimize the systems reversibility. The Ga to desolved $GaO_3^{3-}$ reaction was shown to be reversible using CV analysis though some slight irreversibility was present. The addition of 0.1M desolved $Ga_2O_3$ to the 6M KOH electrolyte showed improved reversibility and the highest stability, of near one peak current ratios and formal reduction potential values. This finding of $Ga_2O_3$ electrolyte additive was applied to the prototype battery for testing. Additionally, because Zr cloth separators resulted in Ga seepage and shorting the addition of a polypropylene separator was added to the prototype cell to prevent shorting. These improvements provided the first charge discharge tests which showed success. Polarization curves were compared between the new test configuration, that of prior groups and that of a commercial Zn-air battery. The improved cell showed slightly higher discharging voltage and stability relative to the old one though more testing needs to be done for inference to be made. The improved cell also handles better than the Zn-air battery at high current densities indicating faster reaction rate and mass transport in the liquid Ga. Although the cell is still only a prototype, its ability to maintain its potential even at higher current densities surpasses that of commercial Zn-air battery. This is significant due to the Ga-air cell being able to compete with the optimized design of the commercially available Zn-air cell at high currents. When only discharging the Ga battery at low currents the voltage was near its open circuit voltage. The discharge lengths where not extremely long due to limiting factors and work still needs to be done.

Limitations and obstacles such as electrolyte drying, battery shorting and electrolysis if addressed, may allow for a feasible ambient temperature liquid metal battery.

One of the large appeals of a liquid metal-air battery proposed by past MQPs is the high energy density and scalability if incorporated into a flow battery configuration. They hypothesis that this flow configuration would reduce limiting factors however because $Ga_2O_3$ is formed, which creates films and is not liquidus at low temperatures the oxide would likely clog a flowing cell. In this type of cell, the Ga flowing through the reaction area, oxidizing in the process, creates solid oxides which form on and around the reacting area therefore clogging the flow. This problem may be mitigated if the oxides were dissolved into electrolyte however future exploration would need to be done to confirm.

**5.2 Future Work**

Despite the cell having results proving the concept that this kind of battery is feasible, there are still obstacles to be overcome that may be addressed with future research and experimentation. Obstacles such as Ga shorting and poor contact areas include the unlikelihood of a flow battery configuration working as stated before. CV testing may be applied to the prototype cell itself to determine a better understanding of the chemistry taking place in the actual battery cell. Applying CV, linear sweep voltammetry and chronoamperometry to the Swagelok cell future researchers can determine the internal diffusion coefficient of different configurations allowing for further optimization of the system. Additionally, electrolyte additives such as Ga fluoride for basic, or Thiocyanate for acidic electrolytes have shown to improve Ga redox reversibility (Kozin & Gaidin, 2009). Variation of the Swagelok cell components can decrease the internal resistance and improve voltage readout. Running tests in an argon glovebox would also be beneficial to determine oxygen dependence and limiting factors in the absence of oxygen. And finally, calculations of relative cost

vs theoretical energy density of this cell would show if it is a valuable type of battery to pursue. Though even if not economically feasible the value of furthering the understanding and performance of a liquid metal air battery is vital for future research in this area of unexplored high energy density batteries.

# References

**[1]** IPCC, “Global Warming of 1.5oC,” 2014. [Online]. Available: https://www.ipcc.ch/sr15/

**[2]** P. Gu, M. Zheng, Q. Zhao, X. Xiao, H. Xue, and H. Pang, “Rechargeable zinc–air batteries: a promising way to green energy,” vol. 5, no. 17, pp. 7651–7666, 2017.

**[3]** W. M. Saltman and N. H. Nachtrieb, “The Electrochemistry of Gallium,” vol. 100, no. 3, p. 126, 1953, doi: 10.1149/1.2781093.

**[4]** C. K. Das, O. Bass, G. Kothapalli, T. S. Mahmoud, and D. Habibi, “Overview of energy storage systems in distribution networks: Placement, sizing, operation, and power quality,” vol. 91, pp. 1205–1230, 2018.

**[5]** K. Levin, “New Global CO2 Emissions Numbers Are In. They’re Not Good.,” 05-Dec-2018. [Online]. Available: https://www.wri.org/blog/2018/12/new-global-co2-emissions-numbers-are-they-re-not-good

**[6]** OpenStax, *Chemistry*. Rice University, 2016.

**[7]** H. Patrick, Tyler Trettel, Merrill, Laura Christine &. Johnston, Stephen, “A new liquid metal-air battery. ,” 2015 [Online]. Available: https://web.wpi.edu/Pubs/E-project/Available/E-project-043015-010107/restricted/Liquid_Metal-Air_Battery_MQP.pdf

**[8]** “Sources of Greenhouse Gas Emissions.” [Online]. Available: https://www.epa.gov/ghgemissions/sources-greenhouse-gas-emissions

**[9]** A, Marx and Rapoza, K., “Investigation of the Rechargeability of a Liquid Metal-Air Battery,” 2017 [Online]. Available: https://digitalcommons.wpi.edu/mqp-all/4748

**[10]** A. A. Akhil *et al.*, “DOE/EPRI electricity storage handbook in collaboration with NRECA,” 2015.

**[11]** K. M. Abraham, “A brief history of non-aqueous metal-air batteries,” vol. 3, no. 42, p. 67, 2008.

**[12]** M. Pourbaix, “Atlas of Electrochemical Equilibria in Aqueous Solutions, National Association of Corrosion Engineers, Houston, TX,” pp. 384–392, 1974.

**[13]** A. J. Bard and L. R. Faulkner, “Fundamentals and applications,” vol. 2, no. 482, pp. 580–632, 2001.

**[14]** H. Lund and G. Salgi, “The role of compressed air energy storage (CAES) in future sustainable energy systems,” vol. 50, no. 5, pp. 1172–1179, 2009, doi: 10.1016/j.enconman.2009.01.032. [Online]. Available: http://dx.doi.org/10.1016/j.enconman.2009.01.032

**[15]** N. Elgrishi, K. J. Rountree, B. D. McCarthy, E. S. Rountree, T. T. Eisenhart, and J. L. Dempsey, “A Practical Beginner’s Guide to Cyclic Voltammetry,” vol. 95, no. 2, pp. 197–206, Feb. 2018, doi: 10.1021/acs.jchemed.7b00361. [Online]. Available: http://dx.doi.org/10.1021/acs.jchemed.7b00361

**[16]** “Liquid Metal+ Battery,” 2019. [Online]. Available: http://ambri.com/technology/#high-temperature-chemistry

**[17]** “Global energy demand rose by 2.3% in 2018, its fastest pace in the last decade,” 26-Mar-2019. [Online]. Available: https://www.iea.org/news/global-energy-demand-rose-by-23-in-2018-its-fastest-pace-in-the-last-decade

**[18]** M. Truffer, “Purchase 100% truly new renewable electricity,” 2006. [Online]. Available: https://www.globalcarbonproject.org/carbonneutral/NewRenewable.htm

**[19]** “Cyclic Voltammetry: The Basics.,” 2019. [Online]. Available: https://www.ossila.com/pages/cyclic-voltammetry. [Accessed: 2020]

**[20]** Hu, V. W., Vu, H. B., & Zargorski, J., “Liquid Metal-Air Battery for Energy Storage. ,” 2016 [Online]. Available: https://digitalcommons.wpi.edu/mqp-all/4396X

**[21]** M. Skyllas-Kazacos, M. H. Chakrabarti, S. A. Hajimolana, F. S. Mjalli, and M. Saleem, "Progress in Flow Battery Research and Development," vol. 158, no. 8, p. R55, 2011, doi: 10.1149/1.3599565.

**[22]** Y. Nishi, "Lithium ion secondary batteries; past 10 years and the future," vol. 100, no. 1, pp. 101–106, 2001, doi: 10.1016/S0378-7753(01)00887-4. [Online]. Available: http://dx.doi.org/10.1016/S0378-7753(01)00887-4

**[23]** "U.S. energy facts explained," 07-May-2020. [Online]. Available: https://www.eia.gov/energyexplained/us-energy-facts/

**[24]** "Technologies of Energy Storage." [Online]. Available: https://energystorage.org/why-energy-storage/technologies/

**[25]** R. C. Gough *et al.*, "Self-Actuation of Liquid Metal via Redox Reaction," vol. 8, no. 1, pp. 6–10, Jan. 2016, doi: 10.1021/acsami.5b09466. [Online]. Available: http://dx.doi.org/10.1021/acsami.5b09466

**[26]** "Load Shifting (Demand Reduction)," 2016. [Online]. Available: http://fireflyenergy.com/applications/load-shifting-demand-reduction/. [Accessed: 10-Nov-2019]

**[27]** A. . Dehghani-Sanij, E. Tharumalingam, M. . Dusseault, and R. Fraser, "Study of energy storage systems and environmental challenges of batteries," vol. 104, pp. 192–208, Apr. 2019, doi: 10.1016/j.rser.2019.01.023. [Online]. Available: http://dx.doi.org/10.1016/j.rser.2019.01.023

**[28]** "The Longest-Range Electric Vehicle Now Goes Even Farther," 23-Apr-2019. [Online]. Available: https://www.tesla.com/blog/longest-range-electric-vehicle-now-goes-even-farther

**[29]** K. Green, "Analytical Chemistry. Cyclic Voltammetry (CV). ," 2017 [Online]. Available: https://www.jove.com/science-education/5502/cyclic-voltammetry-cv

**[30]** Bio-Logic., "EC-Lab Software User's Manual Version 10.38," 2014. [Online]. Available: https://mmrc.caltech.edu/BioLogic Echem/ECLab Manuals/EC-Lab software user's manual.pdf

**[31]** C. Eaker, M. Khan, and M. Dickey, "A Method to Manipulate Surface Tension of a Liquid Metal via Surface Oxidation and Reduction," no. 107, 2016, doi: 10.3791/53567.

**[32]** Khan, M. R., Eaker, C. B., Bowden, E. F., & Dickey, M. D. "Giant and switchable surface activity of liquid metal via surface oxidation" Proceedings of the National Academy of Sciences of the United States of America, 2014, 111(39), 14047–14051. doi:10.1073/pnas.1412227111

**[33]** L. Otaegui *et al.*, "Performance and stability of a liquid anode high-temperature metal–air battery," vol. 247, pp. 749–755, Feb. 2014, doi: 10.1016/j.jpowsour.2013.09.029.

**[34]** I. L. Koutsopoukos. Hatzi, V. &. Tassiulas, "Optimal energy storage control policies for the smart power grid. ," 211AD. [Online]. Available: https://ieeexplore.ieee.org/abstract/document/6102369

**[35]** J. Matyás, T. Ohji, and X. Liu, Eds., *Advances in Materials Science for Environmental and Energy Technologies II : Ceramic Transactions, Volume 241*. Somerset: John Wiley & Sons, Incorporated, 2013.

# Appendix: A Potentiostat Set Up

Figure 33. shows the electrode leads connected the potentiostat. The White denotes the reference electrode, blue-counter electrode, and red-working electrode. Alligator Clip insulated electrical cables connected the leads to the electrodes in use. Care was taken not to let clips to touch foil table or one another.

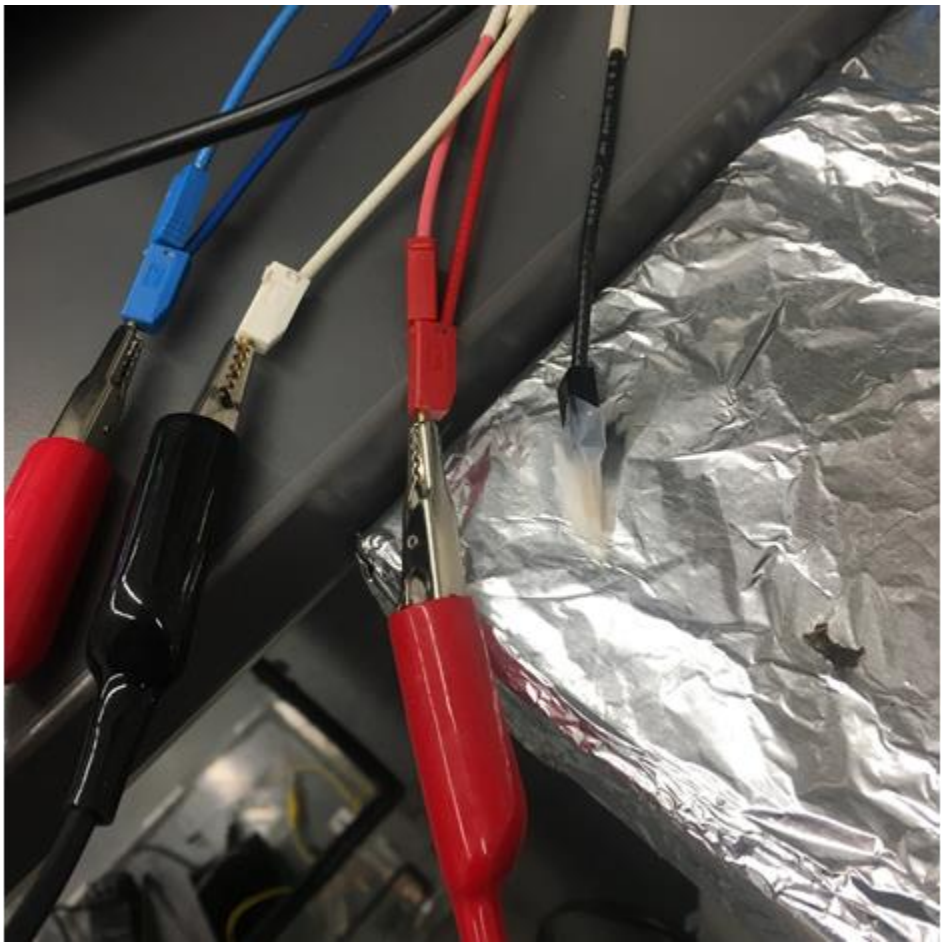

**Figure 33**. Colored electrode connections to potentiostat.

In figure 34 to the right is the small Swagelok cap which was cut to contain the Ga droplet during cycling tests. In the center is the Graphite rod counter electrode a nickel wire was connected

to this with conductive silver cement and then held in place with a nonconductive epoxy (the gray/white shown). The tip was sharpened in case use as a working electrode was desired, but this is unnecessary. On the left is the Pt wire electrode made by EG&G PARC Princeton Research (RDE0021) this was wrapped in Teflon plumbing tape (white) to prevent exposed Pt reacting with electrolyte.

**Figure 34.** Electrodes used in CV test.

Figure 35. Shows the three electrodes held with equal spacing within a beaker on top of a hot plate set at (~50 $^{o}$C) to maintain Ga at a liquid state.

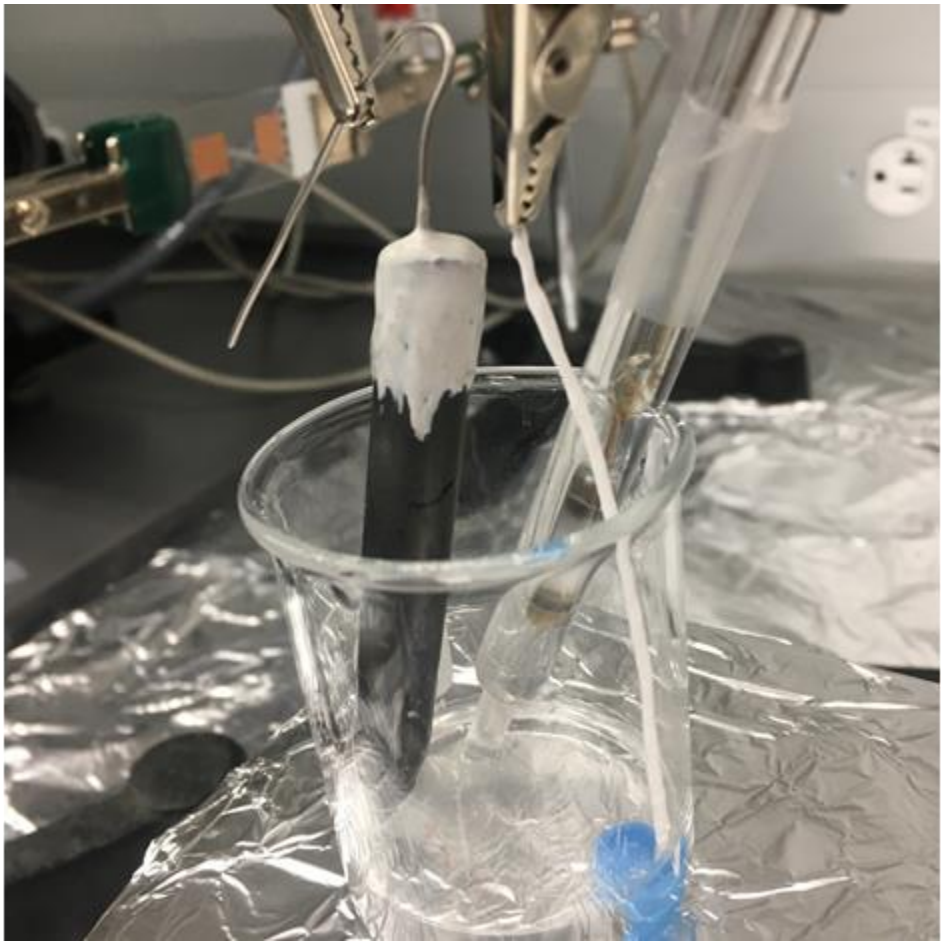

**Figure 35.** Three electrode beaker-cell on hot plate.

# Appendix B: EC Labs Settings

Using EC-Labs software to interface with the potentiostat CV test were run with the three electrode CV program.

**CV:**

Scan rate 0.01v/s-50v/s. Switching potentials were typically -1.7 to -1.2 V vs SCE or -3 to -2 V vs SCE for very wide scans. The number of samples over which the data was averaged was varied depending on the scan rate. At high scan rates each data point was taken individually while at slow scan rates the values were typically averages so that each cycle stayed consistently with 500-1200 samples per cycle.

**For electrodeposition:**

The GCPL2 setting was used as it allows charging with the presents of a reference electrode to evaluate electrode voltages relative to.

Cycle Definition : Charge/Discharge alternance
Initially there was a pause for 1 second. Then a discharge for 30 seconds as it is required with current = -1mA. Then charge for 1hr a 1mA, Potential limitations were wide enough not to interfere with charging or discharging -4 to +4V.

# Appendix C: Swagelok Cell Setup

Figure 39 shows the setup of Swagelok Cell when tests were conducted using the prototype cell. In this image, the positive terminal red alligator clips are attached to a copper ring which sits on the Ga anode side of the cell and the negative/ground terminal black alligator clips also are attached to a copper wire which is connected to the Oxygen cathode side. The whole cell is placed in clamps fitted on a ring stand and is placed underneath a heat lamp with the cell positioned such that the cell is approximately 50 C. Out of the image is the BA500WIN Battery Metric connected to a desktop computer with an external fan due to the internal fan being broken. For the discharge programs, which included the varying separators and Nitrogen sparging tests, the program consisted of an initial pause step followed by 20 second discharge steps with increasing current ranging from 0.1 mA to 15mA with 0.1 mA intervals going to 5mA then 0.5 mA steps afterwards. Afterwards, the program went to a second pause step and was followed by a straight discharge step at 5 mA with a voltage cutoff of 0.1 V. For the Charge/Discharge programs, the program started with an initial pause step followed by a discharge at 5mA for an hour or until a 0.3 V cutoff was reached and then was charged at 5 mA for an hour and this was repeated for a total of three cycles.

**Figure 36.** Swagelok Cell attached to BA500WIN Battery Metric

Figure 37 shows the set up for the cell when running the Nitrogen sparging and limited air flow tests. For these programs, a tube was run from a tank of Nitrogen gas to a smaller tank for excess storage, then a tube was run to a T-splitter where it branched to the hole in the cathode of the cell and was sealed using gaff tape and a beaker containing water for visibly measuring air flow due to speed of gas bubbles. Both the Nitrogen sparging and limited air flow programs used this same setup with Nitrogen being run through the system except for the limited air flow, there was no gas flow, so the tubes provided a makeshift air cutoff.

**Figure 37.** Nitrogen Sparge and Limited Air Flow Set-up

**Figure 38.** Set up of Prototype Cell

**Figure 39.** Deconstructed Swagelok Cell showing Ga seepage around the separators and coil.

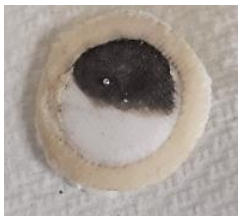

**Figure 40**. Area of contact between Ga and separator

**Figure 41.** Dried KOH on outside of Oxygen cathode after discharge program

**Figure 42.** Gelled KOH accumulate from seeping through separators

**Appendix C1**

Results from varying separator test without oxygen present.

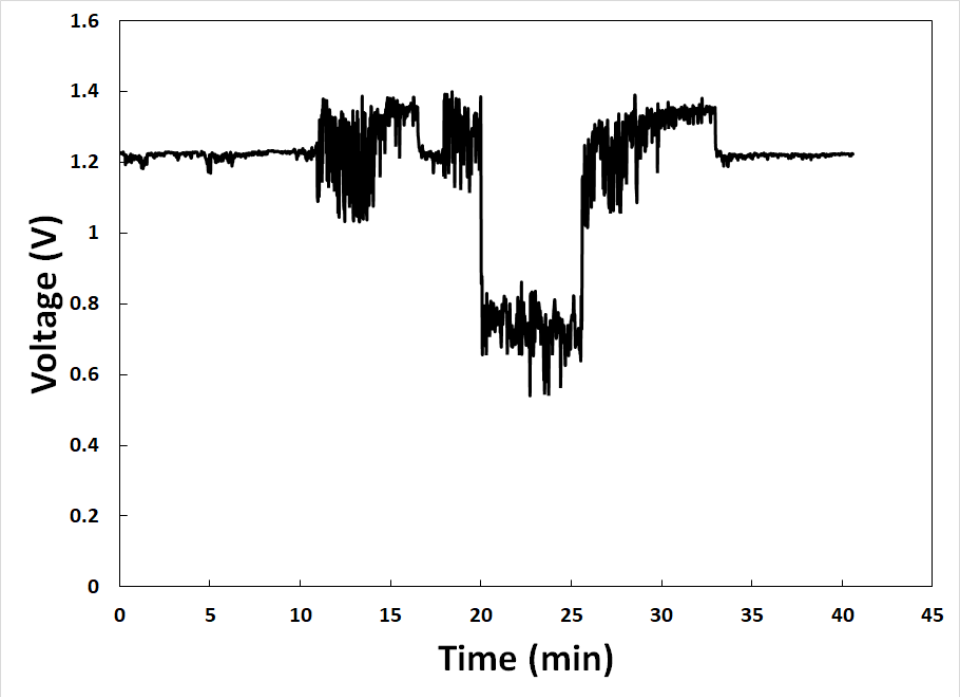


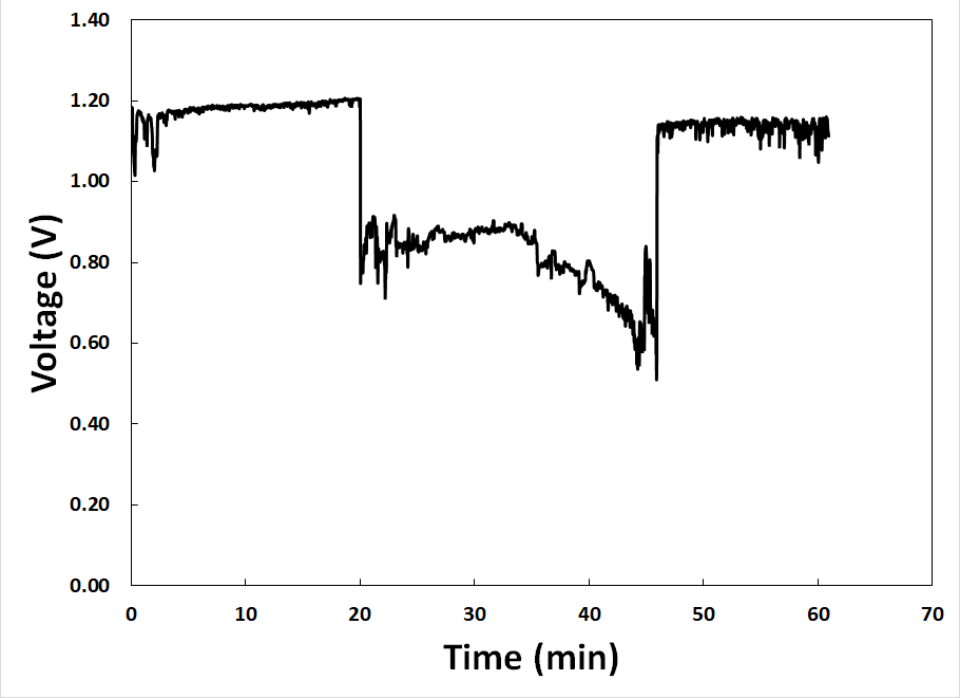

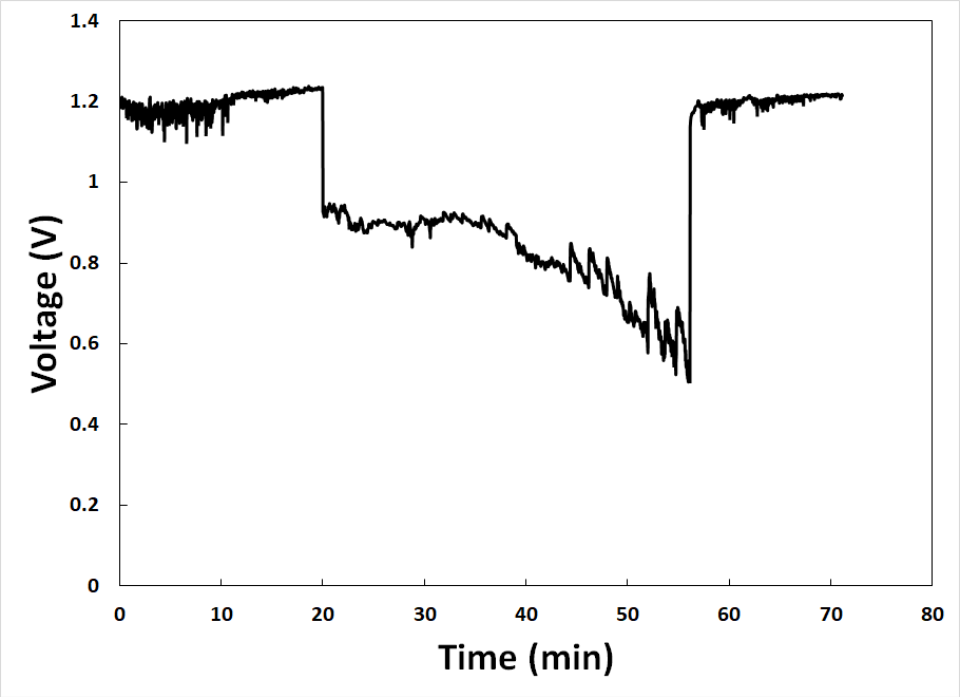


**Figure 43.** Cell in a without air flow with increasing quantity of ZC separators. **Top.** 1 ZC separators. **Middle.** 2 ZC separators. **Bottom.** 3 ZC separators.

# APENDIX D

Example calculations to evaluate the thickness of a film of $Ga_2O_3$ formed during discharge assuming maximum dissolution of $Ga_2O_3$ is ~0.1M in 6M KOH which was approximated experimentally. Using the results from section 4.3.4: 0.00011728 L of KOH/2-separators in a cell combined with the dissolution assumption gives 0.00001173 mols of $Ga^{3+}$soluble in available electrolyte. From section 4.3.5: 0.000086807mols of Ga reacted during discharge. To calculate the remaining undissolved $Ga_2O_3$ subtracting the two quantities above gives 0.00007513 mols Ga. Using the density and molar weight of $Ga_2O_3$ the volume of undissolved $Ga_2O_3$ can be calculated to be $0.00218675\ cm^3$.

To evaluate the volume of pure Ga after oxidation by subtracting the initial amount of Ga from the amount reacted gives a volume of $0.00218675\ cm^3$ remaining pure Ga. Solving for the radius of the pure Ga droplet assuming it is spherical gives r = 0.36413cm. To calculate the thickness of the remaining oxide film the total volume and radius of the remaining droplet was calculated assuming a spherical droplet.

$$(1.2g - 0.000086807molGa \times \frac{69.723gGa}{1molGa}) \times \frac{1cm^3}{5.904gGa} = 0.202227cm^3 = \frac{4}{3}\pi\, r^3$$

$$r = 0.36413cm$$

The thickness of remaining oxide film was calculated by combing the volume of remaining Ga and $Ga_2O_3$ to give $0.00218675\ cm^3 + 0.202227cm^3 = \frac{4}{3}\pi\,(0.36413 + dr)^3$

dr = 0.0013078 cm or 13.1 μm film thickness combining this with the bonded diameter of a $Ga_2O_3$ molecule, assuming its standard density d=$4.5194 \times 10^{-8}$cm. and lastly combing the diameter of

$Ga_2O_3$ with the film thickness to determine the Number of layers of $Ga_2O_3$ required in this ideal case

$\frac{0.0013078\ \text{cm}}{4.5194 \times 10^{-8}\text{cm}}$ = 28940 number of $Ga_2O_3$ layers assuming uniform spherical distribution.